Contrib Mineral Petrol (2002) 144: 257–273
DOI 10.1007/s00410-002-0397-y

ORIGINAL PAPER

Kirill Shmulovich · Wilhelm Heinrich
Peter Möller · Peter Dulski

Experimental determination of REE fractionation between liquid and vapour in the systems NaCl–H_2O and $CaCl_2$–H_2O up to 450 °C

Received: 24 June 2002 / Accepted: 1 July 2002 / Published online: 10 September 2002

Abstract Fractionation of selected REE between brine and vapour was experimentally determined using a large-volume rocking Ti-autoclave that allowed quasi-isobaric sampling of liquid–vapour pairs. Samples were extracted along the 350, 400 and 450 °C-isotherms of the H_2O–NaCl system, and along the 400 °C isotherm of the $CaCl_2$ system. Total salt concentrations were either 6.6 and 10 wt% NaCl or $CaCl_2$, respectively, and total REE concentrations were about 2 ppm of each REE. Starting pH at room temperature was 1.8, added as HCl. In another series of experiments, REEs were added in amounts of 312 ppm. Here, the starting pH at room temperature was 0.5, added as HNO_3:HCl = 1:2. Liquid–vapour pairs (L–V) were analysed for REE by ICP-MS methods. L–V-partitioning of REE along a particular isotherm follows broadly the partitioning of the main salt components, NaCl or $CaCl_2$. $D_{REE} = REE^V/REE^L$ decrease rapidly from the critical point with decreasing pressure (equivalent to increasing salinity of the liquid) as the solvus opens. This is independent of the total amount of the added REE. Log D_{REE} values show approximately linear correlations with decreasing pressure from the critical point to salt-saturated conditions where the L–V curve meets the liquid + vapour + solid boundary. At given P and T, we found a systematic variation of D_{REE} along the La–Lu suite. HREE are enriched in the vapour phase relative to LREE. Fractionation coefficients $K_D = (HREE^V/HREE^L)/(LREE^V/LREE^L)$ increase linearly with $\Delta P = P_{crit}–P$ along a particular isotherm. At the 450 °C isotherm, K_D (Lu/La) at the critical point (425 bar and 10 wt% NaCl) is 1; about 2.5 at 350 bar (33 wt% NaCl in the liquid); and about 5 if extrapolated to salt-saturation (250 bar and 52 wt% NaCl in the liquid). The REE fractionation behaviour is similar along the $CaCl_2$–H_2O solvus boundaries. Existing equations of state and thermodynamic databases of REE species cannot predict this behaviour at L–V-equilibrium conditions. That HREE are preferentially fractionated over LREE into the vapour phase has important petrogenetic consequences. In boiling hydrothermal systems, brines will be depleted in HREE relative to LREE. Isobaric cooling is ineffective for fractionation because the solvus closes and the system eventually shifts into the one-phase field. Fractionation is most effective in systems undergoing isothermal or adiabatic decompression. In an open system, where vapour may escape through cavities, fractionation is probably controlled by a Rayleigh fractionation process, resulting in larger overall fractionation effects. Similar fractionations probably occur during magma degassing at very shallow intrusion levels.

K. Shmulovich · W. Heinrich (✉) · P. Möller · P. Dulski
GeoForschungsZentrum Potsdam,
Experimental Petrology/Geochemistry,
Telegraphenberg, Potsdam, Germany
E-mail: whsati@gfz-potsdam.de
Tel.: +49-331-2881410
Fax: +49-331-2881402

Editorial responsibility: J. Hoefs

Introduction

Rare earth elements (REE) are very useful tracers for a wide variety of geochemical processes. A large and still expanding database exists on REE partition coefficients between coexisting minerals, melts and fluids. Recent developments demonstrated that the controls of REE and trace element partitioning between minerals and melts can be described by the Blundy and Wood (1994) lattice strain model for some important minerals, and the effects of pressure, temperature and composition on mineral-melt partitioning are now quite well understood. Because the REE patterns for each phase and their P–T–*X* dependencies are known, the most important fractionation processes within the Earth's crust and upper mantle, namely partial melting and fractional crystallization, might now be interpreted quantitatively.

Another important fractionation process for elements and isotopes is liquid–vapour separation or 'boiling'. This plays an essential role in hydrothermal ore deposits

around igneous bodies that intruded into shallow levels of the crust and also in mid-ocean ridge vents. Fluids in these environments are usually brines with NaCl, KCl and $CaCl_2$ as main solutes. Fluid immiscibility has been demonstrated by a large number of fluid-inclusion studies (Roedder 1984, for an early compilation). Aside from the main components, experimental studies on liquid–vapour fractionation in water–salt systems have mainly concentrated on D/H, $^{11}B/^{10}B$ and $^{18}O/^{16}O$ stable isotope partitioning (Spivack et al. 1990; Horita et al. 1995; Berndt et al. 1996; Driesner 1997a, 1997b; Shmulovich et al. 1999), or on partitioning of alkalis and halogenides (Berndt and Seyfried 1997). Recently, LA-ICP-MS microanalysis of coexisting natural brine and vapour inclusions that were homogeneously trapped on the L–V solvus boundaries provided partition coefficients for a large number of trace elements (Heinrich et al. 1999). These are, however, mostly semiquantitative because the pressure–temperature relationships that define the solvi are not exactly known for these natural systems. Surprisingly, little attention has been given to fractionation of the REE between liquid and vapour and, up to now, there are no data available neither for experimental nor for natural systems.

Numerous fluid inclusion studies have shown that the salinities of brines in liquid–vapour systems may strongly vary from low salinity up to salt-saturated conditions. The L–V solvus of H_2O–salt systems in P–T–X space expands rapidly with increasing temperature and salt concentration (Sourirajan and Kennedy 1962; Bischoff and Pitzer 1989; Shmulovich et al. 1995a; Bischoff et al. 1996). Vapour exsolution from brines flowing through shallow hydrothermal systems is a common process induced by isobaric heating or adiabatic decompression. If significant differences in the REE fractionation behaviour along the La–Lu suite between liquid and vapour exist, this would impose contrasting REE patterns on the two fluid phases. Large overall fractionations are then expected because vapour exsolution is mainly controlled by Rayleigh fractionation.

In this contribution, we present experimentally determined fractionation data of selected REE between liquid and vapour along the 350, 400 and 450 °C isotherms in the matrix systems NaCl–H_2O and $CaCl_2$–H_2O. We derive pressure- and salinity-dependent partition coefficients for each of the REE, and show that L–V fractionations change systematically along the La–Lu suite. Finally, we discuss possible consequences for the REE concentrations in late-stage magmatic and hydrothermal minerals and speculate how REE patterns of minerals and rocks could be misinterpreted if boiling is ignored.

Experimental and analytical techniques

Large-volume Ti-autoclave

The experiments have been performed using a high-temperature rocking autoclave of about 500 cm^3 volume. The device is described in detail by Shmulovich et al. (1999). All parts in contact with the fluids including capillary tubes and sample containers are made of Ti-alloy (BT-8). The inner surface of the autoclave, sampling lines and valves were passivated with 20% nitric acid at 400 °C. SEM observations showed a stable protective layer of TiO_2. The large volume allows quasi-isobaric sampling of coexisting liquid and vapour through capillary tubes at different ends of the autoclave. The dead, non-heated volume of the capillary, valve and pressure transducer systems was about 0.05 cm^3. About 1 cm^3 liquid and 1.4 cm^3 vapour were drawn off for each liquid–vapour pair. Thus, the sample volume was only about 0.3% of the total, and the dead volume about 0.5% of the sample volume. The autoclave was heated by three independently controlled furnaces resulting in a maximum thermal gradient of 0.5 °C inside the vessel. The maximum error in the temperature accuracy is better than ±2 °C. Pressure was measured on-line using a transducer gauge with a sensitivity of about 0.5 mV/bar calibrated at the liquid–vapour boundaries of pure water. Pressure uncertainty is better than ±1.5 bar.

Starting solutions

Experiments on liquid–vapour fractionation in the pure NaCl–H_2O and $CaCl_2$–H_2O systems have shown that hydrolysis plays an important role and increases with increasing opening of the solvus. In the NaCl–H_2O system, the quench-pH of vapour may reach down to values of 3, that of coexisting brine up to 11 (Fournier 1987; Vakulenko et al. 1989; see also Fig. 8.9 in Shmulovich et al. 1995a). A similar behaviour occurs in the $CaCl_2$–H_2O system, where hydrolysis is prominent at pressures below 250 bar, eventually causing precipitation of $Ca(OH)_2$ from the alkaline brine (Bischoff et al. 1996). This effect could possibly result in precipitation of REE-hydroxides in our experiments. In order to prevent hydroxide precipitation a high acidity for the starting solutions was chosen. Three sets of experiments were performed.

For the NaCl–H_2O system two different starting solutions were prepared. For the first, we applied commercial standard REE-solutions, which were 0.32 molar in HNO_3. An aliquot of 20 g of NaCl was added to 100 ml of solution having 1,000 µg/ml La, Gd and Lu. The resulting solution contained 312 ppm of Gd, La and Lu, and 6.6 wt% NaCl (= 1 mol/kg), yielding a pH of 0.5 at room temperature. The second solution contained 10 wt% NaCl and about 2 ppm of La, Ce, Eu, Gd, Y, Ho and Lu, added as $REECl_3$. The pH of 1.8 at room temperature was adjusted with HCl.

Experiments on the $CaCl_2$–H_2O–HCl system started with a homogeneous solution of 10 wt% $CaCl_2$ and a pH of 1.8, adjusted with HCl. La, Ce, Eu, Gd, Y, Ho and Lu were mostly added as $REECl_3$ in 2% HCl solution in amounts of about 2 ppm for each REE. Analysis of the starting solution revealed the presence of 4.9 ppm Sr introduced as an impurity from the used $CaCl_2$. L–V fractionation of Sr could, therefore, be determined as a byproduct.

Sampling strategy

The sampling procedure was to extract liquid–vapour pairs at a particular isotherm at different pressures. For that, the vessel was evacuated through one capillary and filled through the other with about 300 cm^3 of homogeneous starting solution. The autoclave was then heated up to the particular isotherm of interest. The amount of initial solution was chosen in such a way that the experiment started off with a homogeneous one-phase fluid above the critical pressure for the particular composition of the fluid. Some of the charge was subsequently extracted and the two-fluid solvus was intersected by the concomitant pressure drop. Before sampling, the vessel was kept in a horizontal position for about 24 h. The autoclave was then turned to an inclined or vertical position and valves were opened for 10 to 15 s. Fluids in amounts of 1 cm^3 (liquid) and 1.4 cm^3 (vapour) were trapped in ice-cooled Ti-containers. At the vapour line, the first 0.2 cm^3 were always discarded. Subsequently, more gas was drawn off the vapour line, and the procedure was repeated isothermally at a particular lower pressure,

equivalent to a higher salinity of the fluid. The identical procedure was then applied for another isotherm.

It is important to note that for any particular isotherm, the pressure release, i.e. fluid extraction from the homogeneous supercritical fluid to the first sampled liquid vapour pair, occurred in a somewhat uncontrolled manner. Large amounts of fluid are rapidly drawn off at the beginning, and equilibrium between liquid and vapour is possibly not maintained during this stage of the experiment. This implies that the mass balance between matrix elements and REE from the starting solution to the first liquid–vapour pair must not necessarily work out exactly. Sampling of each liquid–vapour pair, however, occurred under equilibrium conditions (see below).

Analytical procedure

For REE determination, weighted aliquots of liquid and vapour were diluted with 0.5 M HCl by factors of 1,000 (liquid) and 100 (vapour). Ru and Re were added in concentrations of 10 ng/ml for shift corrections in ICP-MS analysis. REEs were measured with a precision of about 2%. The accuracy is better than ±5%. For determination of Na and Ca, aliquots of liquid and vapour were diluted by factors of 500 and 3, respectively. Both elements were determined by AES using matrix-adjusted standards. Chloride was titrated after Mohr. About 200 µl of the original solution was diluted to about 10 ml. The solution was then adjusted to pH >5 and $KCrO_4$ added as indicator. The vapour was titrated with 0.02, and the liquid with 0.1 mol $AgNO_3$. The titration is finished when the red-brown colour of $AgCrO_4$ is stable. Determinations of Cl^- in known NaCl solutions proved that the accuracy and precision of the titration procedure is about 5%.

pH measurements of quenched liquids and vapours of the NaCl-bearing systems were performed directly in aliquots of the solution using a pH-sensitive electrode. The liquid of the $CaCl_2$-bearing system was diluted by a factor of 100 before measurement. The salinity of the liquids is generally high, which leads to salt effects that alter the pH values during determination with the electrode. To correct that, an H_2O–HCl solution of pH 1.8 was mixed with various amounts of NaCl and $CaCl_2$, respectively, up to salt saturation conditions. Measurements of these solutions show that the measured pH strongly depends on increasing salinity. A correction curve for different salinities was established and the measured pH values of the liquids adjusted to that. The errors of the given pH values at very high salinities might be as high as 10%. The salinity of most vapour phases is low and a correction for the salt effect on pH was only necessary for a few vapour samples. In order to obtain the molalities of the fluids, their densities were determined by weighing 0.1 ml of each fluid sample. Measured concentrations of major and trace elements were recalculated to molalities (mol/kg) and ppm (µg/g), respectively, using measured densities.

Results

The analytical results are given in Tables 1, 2 and 3. The analytical precision is checked by balancing the cation and anion equivalents calculated from values in Tables 1, 2 and 3. In sampled liquids, the balance is controlled within 10% of either the anions or the cations, which is expected from the types of analyses applied. There is a slight deficit in anions for liquids for the HNO_3-bearing system (Table 1) because NO_3^- was not analysed. In all experiments, vapours have always a cation deficit due to hydrolysis and preferred fractionation of HCl into vapour (see below).

Table 1 Element concentrations in coexisting liquid and vapour at different pressures for the 450 °C isotherm of the NaCl–H_2O–HCl(–HNO_3) system, along with partition coefficients $D = REE^{vapour}/REE^{liquid}$ and distribution coefficients $K_D = (REE^{vapour}/REE^{liquid})/(La^{vapour}/La^{liquid})$. The homogeneous starting solution was 1.06 mol NaCl, had 312 ppm REE each, and a pH of 0.5

Run no.	R1	R2	R3	R4	R5	R6	R7	R8	R9	R10[a]
Liquid										
Pressure (bar)	426	427	417	415	400	395	379	377	362	359
Density (g/ml)	1.11	1.111	1.13	1.13	1.16	1.16	1.193	1.205	1.218	1.174
La (µg/g)	480	509	593	598	682	722	821	873	915	754
Gd	490	518	617	609	708	743	850	909	951	761
Lu	458	482	569	566	655	693	798	849	895	724
Na (mol/kg)	2.05	2.14	2.49	2.49	2.89	3.04	3.48	3.70	3.82	3.24
Cl (mol/kg)	1.99	2.06	2.32	2.41	2.72	2.82	3.17	3.30	3.47	2.97
pH	0.7	0.7	0.9	0.9	1.0	1.0	1.1	1.1	1.1	1.5
Σan–Σcat	–0.06	–0.08	–0.16	–0.08	–0.17	–0.22	–0.31	–0.40	–0.35	–0.28
Vapour										
Pressure (bar)	427	428	419	417	403	398	382	379	366	362
Density (g/ml)	1.04	1.04	1.03	1.03	1.02	1.02	1.014	1.011	1.008	1.008
La (µg/g)	110	80	45	30	8.7	7.4	2.3	2.2	1.0	1.1
Gd	123	92	54	38	12	11	3.7	3.5	1.7	1.7
Lu	118	91	55	41	14	13	4.7	4.4	2.3	2.2
Na (mol/kg)	0.086	0.072	0.053	0.044	0.023	0.021	0.0120	0.0110	0.0078	0.0072
Cl (mol/kg)	0.097	0.085	0.068	0.062	0.045	0.041	0.032	0.030	0.027	0.026
pH	0.3	0.4	0.4	0.4	0.4	0.4	0.5	0.5	0.5	0.5
Σan–Σcat	0.011	0.014	0.015	0.018	0.021	0.020	0.020	0.019	0.019	0.019
D (REE^V/REE^L)										
La	0.23	0.16	0.076	0.051	0.013	0.010	0.0028	0.0025	0.0011	0.0014
Gd	0.25	0.18	0.087	0.063	0.017	0.014	0.0043	0.0038	0.0018	0.0022
Lu	0.26	0.19	0.097	0.073	0.022	0.018	0.0059	0.0052	0.0026	0.0031
K_D [$(REE/La)^V/(REE/La)^L$]										
Gd/La	1.09	1.13	1.15	1.24	1.36	1.38	1.54	1.51	1.58	1.60
Lu/La	1.12	1.21	1.27	1.43	1.73	1.77	2.07	2.03	2.31	2.20

[a]Liquid supersaturated in NaCl at room conditions, which caused salt precipitation

Table 2 Element concentrations in coexisting liquid and vapour at 450, 400 and 350 °C and different pressures of the NaCl–H_2O–HCl system, along with partition coefficients $D = REE^{vapour}/REE^{liquid}$ and distribution coefficients $K_D = (REE^{vapour}/REE^{liquid})/(La^{vapour}/La^{liquid})$. The homogeneous starting solution had 10 wt% NaCl, 2 ppm of each REE and pH 1.8

Run no.	5	6	3	4	8	9	10	7	11	12	13
Temperature (°C)	450	450	400	400	400	400	400	350	350	350	350
Pressure (bar)	410	383	260	255	248	243	242	146	141	137	133
Liquid											
Density (g/ml)	1.11	1.15	1.08	1.09	1.11	1.13	1.14	1.09	1.11	1.13	1.15
La (μg/g)	0.62	0.73	1.23	1.26	1.17	1.02	0.87	1.52	1.43	1.46	1.28
Ce	0.052	0.052	0.13	0.127	0.166	0.104	0.075	0.560	0.415	0.289	0.17
Eu	0.38	0.44	0.95	0.96	0.79	0.61	0.47	1.23	1.01	0.90	0.69
Gd	0.48	0.57	1.19	1.16	0.98	0.75	0.59	1.47	1.22	1.10	0.84
Y	0.32	0.35	0.93	0.93	0.68	0.52	0.36	1.20	0.96	0.81	0.59
Ho	0.33	0.36	0.91	0.91	0.69	0.50	0.37	1.17	0.89	0.75	0.54
Lu	0.33	0.35	0.96	0.96	0.66	0.47	0.33	1.25	0.90	0.71	0.48
Na (mol/kg)	2.28	2.93	1.82	1.87	2.31	2.66	2.57	1.94	2.25	2.62	2.96
Cl (mol/kg)	2.27	2.91	1.82	1.86	2.30	2.61	2.78	1.94	2.22	2.60	2.91
pH	1.6	2.0	1.9	1.9	2.0	2.2	2.2	2.0	1.9	2.2	2.1
Σan–Σcat	–0.01	–0.02	0.00	–0.01	–0.01	–0.05	0.21	0.00	–0.02	–0.02	–0.04
Vapour											
Density (g/ml)	1.03	1.016	1.013	1.018	1.011	1.01	1.006	1.003	1.01	1.01	1.007
La (μg/g)	0.066	0.020	0.043	0.129	0.046	0.008	0.004	0.041	0.022	0.014	0.0016
Ce	0.006	0.002	0.004	0.014	0.012	0.006	0.001	0.014	0.014	0.004	0.0004
Eu	0.046	0.012	0.028	0.097	0.030	0.002	0.002	0.032	0.014	0.011	0.0009
Gd	0.066	0.021	0.050	0.124	0.042	0.006	0.004	0.045	0.019	0.015	0.0016
Y	0.042	0.011	0.030	0.094	0.025	0.002	0.001	0.030	0.011	0.011	0.0006
Ho	0.043	0.012	0.029	0.090	0.027	0.002	0.002	0.031	0.013	0.010	0.0007
Lu	0.057	0.021	0.054	0.103	0.039	0.005	0.004	0.043	0.017	0.012	0.0016
Na (mol/kg)	0.583	0.243	0.046	0.227	0.084	0.027	0.017	0.025	0.028	0.002	0.0004
Cl (mol/kg)	0.603	0.268	0.064	0.267	0.118	0.049	0.044	0.072	0.066	0.027	0.018
pH	1.6	1.6	1.4	1.4	1.4	1.5	1.5	1.2	1.3	1.5	1.6
Σan–Σcat	0.020	0.025	0.018	0.040	0.034	0.022	0.027	0.047	0.039	0.025	0.018
D (REE^V/REE^L)											
La	0.11	0.027	0.035	0.103	0.039	0.008	0.005	0.027	0.015	0.010	0.0012
Eu	0.12	0.028	0.029	0.101	0.038	0.003	0.004	0.026	0.014	0.012	0.0013
Gd	0.14	0.036	0.042	0.106	0.043	0.008	0.006	0.030	0.016	0.014	0.0019
Y	0.13	0.032	0.032	0.101	0.037	0.004	0.004	0.025	0.011	0.013	0.0010
Ho	0.13	0.032	0.032	0.099	0.040	0.004	0.005	0.027	0.014	0.014	0.0013
Lu	0.18	0.059	0.057	0.11	0.058	0.011	0.012	0.035	0.019	0.016	0.0033
K_D $[(REE/La)^V/(REE/La)^L]$											
Gd/La	1.27	1.34	1.20	1.04	1.08	0.98	1.36	1.14	1.03	1.41	1.54
Lu/La	1.63	2.19	1.62	1.05	1.47	1.43	2.62	1.30	1.25	1.70	2.68

We also checked if the mass balance between matrix elements and REE from the starting solution to the first liquid–vapour pair during pressure release was maintained. The mass balance of the major elements for the first vapour–liquid pair in each set of experiments was calculated applying

$$[El]_{liquid}\varepsilon + [El]_{vapour}(1-\varepsilon) = [El]_{initial} \quad (1)$$

where ϵ is the fraction of liquid in the autoclave at given P–T conditions of the first sampling, and $[El]_{liquid}$, $[El]_{vapour}$ and $[El]_{initial}$ are the measured concentrations of the major elements in liquid and vapour of the first liquid–vapour pair, and the starting solution, respectively. Values for the fraction of liquid calculated for the cations Na and Ca, and also for Cl, are given in Table 4. Mass balance is given if measured REE concentrations in liquid and vapour multiplied with their respective fractions yield about the concentrations of the starting solution. Table 4 shows that this holds for the first L–V pair of series 1 and also of series 3, with the exception of Ce. For series 2 (total concentration is only about 2 ppm), it is obvious that about 50% of each REE were removed from the L–V system. In can reasonably be assumed that REE loss into the autoclave occurred due to incomplete passivation of the walls. The effect is very large for Ce, which is strongly fractionated as CeO_2 into the protective layer. We will show below that adsorption of REE has no significant effect on their distribution behaviour between liquid and vapour.

The system NaCl–H_2O–HCl(–HNO_3)

The 450 °C-isotherm at $pH^{initial}$ 0.5

Liquid–vapour fractionation of La, Gd and Lu have been determined for the 450 °C-isotherm at ten pressures between 427 and 359 bar, along with the matrix elements Na and Cl. The solvus boundaries of the NaCl–H_2O–HCl system are shown in Fig. 1, together with that of pure NaCl–H_2O from Bischoff and Pitzer (1989). Our

Table 3 Element concentrations in coexisting liquid and vapour at different pressures for the 400 °C isotherm of the $CaCl_2$–H_2O–HCl system, along with partition coefficients $D = REE^{vapour}/REE^{liquid}$ and distribution coefficients $K_D = (REE^{vapour}/REE^{liquid})/(La^{vapour}/La^{liquid})$. Starting mixture had 10 wt% $CaCl_2$, 4.9 ppm Sr, about 2 ppm of each REE added as $REECl_3$ and pH 1.8

Run no.	CR1	CR2	CR3	CR4	CR5	CR6	CR7	CR8	CR9	CR10	CR11	CR12	CR13	CR14	CR15
Pressure (bar)	298	295	292	288	285	281	277	272	270	260	253	232	222	218	187
Liquid															
Density(g/ml)	1.12	1.11	1.15	1.16	1.16	1.19	1.20	1.20	1.21	1.25	1.26	1.32	1.37	1.38	1.48
Sr (μg/g)	9.1	8.9	10.1	11.1	12.2	12.9	13.7	14.5	14.9	17.0	18.7	22.3	23.9	24.8	29.5
La	4.65	4.56	5.00	5.55	5.95	6.22	6.19	6.50	6.69	6.81	7.32	5.21	1.50	1.91	2.73
Ce	0.65	0.63	0.63	0.66	0.60	0.56	0.48	0.47	0.48	0.38	0.34	0.18	0.13	0.23	0.15
Eu	3.58	3.51	3.74	4.22	4.30	4.34	4.25	4.41	4.63	4.32	4.51	3.34	1.66	1.73	2.30
Gd	3.87	3.86	4.12	4.64	4.72	4.84	4.67	4.83	5.02	4.69	4.96	3.78	1.94	1.99	2.68
Y	3.42	3.37	3.65	4.00	4.10	4.13	4.08	4.14	4.44	4.11	4.28	3.34	2.18	2.16	2.54
Ho	3.13	3.17	3.33	3.65	3.69	3.68	3.57	3.60	3.83	3.47	3.59	2.55	1.90	1.77	2.06
Lu	2.84	2.90	3.00	3.29	3.25	3.19	3.04	3.07	3.23	2.83	2.84	1.88	1.60	1.42	1.60
Ca (mol/kg)	1.16	1.19	1.34	1.46	1.63	1.70	1.71	1.91	1.76	1.97	2.20	2.43	2.57	2.54	2.86
Cl (mol/kg)	2.29	2.27	2.46	2.73	2.99	3.17	3.28	3.51	3.52	3.88	4.31	4.77	5.00	5.02	5.67
pH	2.2	2.3	2.4	2.5	2.7	2.8	2.8	3.0	2.9	3.2	5.1	7.5	~9	~9	~10
Σan–Σcat	–0.04	–0.11	–0.21	–0.18	–0.28	–0.23	–0.14	–0.31	–0.01	–0.06	–0.09	–0.10	–0.13	–0.07	–0.06
Vapour															
Density(g/ml)	1.02	1.02	1.02	1.02	1.02	1.02	1.02	1.02	1.02	1.02	1.02	1.02	1.02	1.02	1.02
Sr (μg/g)	2.48	2.20	1.32	0.64	0.37	0.19	0.12	0.066	0.059	0.023	0.015	0.0046	0.0066	0.014	0.0068
La	1.11	1.06	0.55	0.24	0.12	0.052	0.031	0.018	0.018	0.0045	0.0043	0.0023	0.0099	0.0013	0.0028
Ce	0.17	0.15	0.072	0.030	0.013	0.0052	0.0032	0.0020	0.0018	0.0007	0.0008	0.0005	0.0115	0.0005	0.0007
Eu	0.95	0.93	0.49	0.23	0.12	0.049	0.028	0.017	0.017	0.0041	0.0039	0.0019	0.0015	0.0010	0.0019
Gd	1.06	1.04	0.56	0.26	0.14	0.057	0.034	0.020	0.020	0.0047	0.0048	0.0024	0.0018	0.0013	0.0022
Y	1.07	1.03	0.56	0.28	0.14	0.060	0.035	0.020	0.020	0.0045	0.0040	0.0018	0.0013	0.0009	0.0010
Ho	0.89	0.87	0.47	0.22	0.12	0.049	0.028	0.017	0.016	0.0042	0.0038	0.0019	0.0014	0.0009	0.0013
Lu	0.87	0.87	0.47	0.23	0.12	0.051	0.030	0.018	0.017	0.0048	0.0049	0.0026	0.0019	0.0015	0.0019
Ca (mol/kg)	0.38	0.34	0.21	0.12	0.079	0.037	0.024	0.015	0.013	0.0055	0.0034	0.0011	0.0006	0.0007	n.d.
Cl (mol/kg)	0.76	0.69	0.44	0.25	0.17	0.10	0.071	0.055	0.049	0.034	0.030	0.024	0.024	0.023	0.025
pH	1.6	1.7	1.7	1.7	1.7	1.7	1.7	1.7	1.7	1.7	1.7	1.7	1.7	1.7	1.6
Σan–Σcat	0.000	0.001	0.011	0.022	0.010	0.025	0.022	0.025	0.023	0.023	0.023	0.022	0.023	0.022	n.d.
$D\ (REE^V/REE^L)$															
Sr	0.27	0.25	0.13	0.058	0.030	0.014	0.008	0.005	0.004	0.001	0.001				
La	0.24	0.23	0.11	0.044	0.021	0.008	0.0049	0.0027	0.0028	0.0007	0.0006				
Ce	0.26	0.24	0.11	0.045	0.022	0.009	0.0066	0.0042	0.0037	0.0018	0.0024				
Eu	0.27	0.27	0.13	0.055	0.027	0.011	0.0067	0.0039	0.0036	0.0010	0.0009				
Gd	0.27	0.27	0.14	0.056	0.029	0.012	0.0072	0.0041	0.0040	0.0010	0.0010				
Y	0.31	0.31	0.15	0.069	0.035	0.015	0.0085	0.0049	0.0045	0.0011	0.0009				
Ho	0.28	0.28	0.14	0.061	0.032	0.013	0.0079	0.0046	0.0043	0.0012	0.0011				
Lu	0.31	0.30	0.16	0.070	0.036	0.016	0.0098	0.0058	0.0054	0.0017	0.0017				
Ca	0.33	0.29	0.16	0.079	0.048	0.022	0.0141	0.0078	0.0074	0.0028	0.0015				
$K_D\ [(REE/La)^V/(REE/La)^L]$															
Ce/La	1.08	1.04	1.04	1.03	1.04	1.12	1.32	1.56	1.34	2.73	4.05				
Eu/La	1.12	1.14	1.19	1.26	1.30	1.35	1.35	1.43	1.31	1.45	1.46				
Gd/La	1.15	1.17	1.23	1.28	1.40	1.41	1.46	1.50	1.45	1.52	1.63				
Y/La	1.30	1.32	1.40	1.57	1.67	1.74	1.72	1.81	1.63	1.69	1.59				
Ho/La	1.19	1.19	1.28	1.39	1.53	1.61	1.59	1.69	1.55	1.84	1.79				
Lu/La	1.29	1.29	1.43	1.59	1.75	1.91	1.97	2.13	1.96	2.60	2.91				
$K_D\ [(REE/Ca)^V/(REE/Ca)^L]$															
La/Ca	0.73	0.81	0.69	0.56	0.43	0.38	0.35	0.35	0.37	0.23	0.38				
Ce/Ca	0.79	0.84	0.71	0.57	0.45	0.43	0.46	0.55	0.50	0.64	1.55				
Eu/Ca	0.81	0.92	0.82	0.70	0.56	0.52	0.47	0.50	0.49	0.34	0.56				
Gd/Ca	0.84	0.94	0.84	0.72	0.60	0.54	0.51	0.53	0.54	0.35	0.62				
Y/Ca	0.95	1.06	0.96	0.87	0.72	0.66	0.60	0.63	0.61	0.39	0.61				
Ho/Ca	0.87	0.96	0.88	0.78	0.66	0.61	0.56	0.59	0.58	0.43	0.68				
Lu/Ca	0.94	1.04	0.98	0.88	0.75	0.73	0.69	0.75	0.73	0.61	1.11				

NaCl concentrations have been calculated assuming that all of the measured Na is present as NaCl. The very acid composition and presence of some HNO_3 of the starting solution shifts the critical point to a higher pressure of about 440 bar relative to the NaCl–H_2O system (423 bar). The limbs of the liquid compositions broadly coincide whereas, at acidic conditions, the NaCl concentration in the vapour within the sampled pressure range is about one order of magnitude lower. The liquid–vapour solvus boundary appears properly constrained and there is no hint of contamination of vapour by liquid or vice versa during sampling.

La, Gd and Lu are enriched in the liquid relative to the starting composition. Concentrations increase linearly with decreasing pressure that is with increasing salinity of the liquid (Fig. 2). At 426 bar, the

Table 4 Liquid–vapour ratios in the autoclave when the first L–V pair for each of the three series is drawn off (R1, 3, CR1, *resp.*). Fraction of liquid was calculated from the concentrations of the major components NaCl and $CaCl_2$ using Eq. (1). Total REE concentrations ($\Sigma L + V$) are calculated from measured REE^L and REE^V applying L–V ratios from major components, and compared with concentrations in the starting solution (in %)

	Experimental series 1 (Table 1)				Experimental series 2 (Table 2)				Experimental series 3 (Table 3)			
	Starting solution	First liquid	First vapour	Fraction of liquid	Starting solution	First liquid	First vapour	Fraction of liquid	Starting solution	First liquid	First vapour	Fraction of liquid
Na (mol)	1.07	2.05	0.086	0.5	1.74	1.82	0.046	0.95				
Ca (mol)									0.715	1.16	0.38	0.43
Cl (mol)	1.07	1.99	0.097	0.52	1.72	1.82	0.064	0.94	1.39	2.29	0.76	0.41
				$\Sigma L + V$ (% start sol.)				$\Sigma L + V$ (% start sol.)				$\Sigma L + V$ (% start sol.)
La (ppm)	312	480	110	298 (95%)	1.93	1.23	0.043	1.17 (61%)	1.89	4.65	1.11	2.60 (137%)
Ce					1.94	0.13	0.004	0.13 (7%)	1.92	0.65	0.17	0.37 (19%)
Eu					1.92	0.95	0.028	0.90 (47%)	1.89	3.58	0.95	2.06 (109%)
Gd	312	490	123	309 (99%)	1.91	1.19	0.050	1.13 (59%)	1.85	3.87	1.06	2.24 (121%)
Y					2.04	0.93	0.030	0.88 (43%)	1.94	3.42	1.07	2.06 (106%)
Ho					1.94	0.91	0.029	0.86 (45%)	1.90	3.13	0.89	1.83 (96%)
Lu	312	458	118	290 (93%)	1.87	0.96	0.054	0.90 (49%)	1.81	2.84	0.87	1.70 (94%)
Sr									4.53	9.10	2.48	5.26 (109%)

concentration of La is 480 ppm, of Gd 490 ppm and of Lu 458 ppm. The pressure drop to 362 bar results in 915 ppm La, 951 ppm Gd and 895 ppm Lu. The pressure–concentration patterns for La, Gd and Lu are almost parallel. The vapour phase is depleted in La, Gd and Lu relative to the starting solution (Fig. 3). Concentrations near the critical point are around 100 ppm at 427 bar (La: 110 ppm; Gd: 123 ppm; Lu: 118 ppm) and drop to values of about 1 ppm at 366 bar (La: 1.1 ppm; Gd: 1.7 ppm; Lu: 2.2 ppm).

The corresponding partition coefficients $D = REE^{vapour}/REE^{liquid}$ are shown in Fig. 4. The accuracy is largely controlled by the sampling procedure of L–V pairs because the fluids were not collected exactly under isobaric conditions. The vapour pressures are 1 to 3 bar higher than the corresponding liquid pressures (Table 1). However, the calculated REE partition coefficients depend mainly on their pressure-dependent concentrations in the vapour phase and are, therefore, determined with sufficient accuracy. Near the critical point at 427 bar, Lu is slightly enriched in the vapour phase relative to Gd and La, but relative fractionation is small ($D_{Lu} = 0.26$; $D_{Gd} = 0.25$; $D_{La} = 0.23$). It becomes more significant as pressure drops with the opening of the solvus. Patterns in Fig. 4 split up in such a way that in the range of 366 to 362 bar $D_{La} \approx 3\times10^{-3}$, $D_{Gd} \approx 2\times10^{-3}$ and $D_{Lu} \approx 1\times10^{-3}$. If the three curves are tentatively extrapolated to the D-value of 1 (dashed line in Fig. 4) they coincide at 447 ± 4 bar and define the critical point of our system at $pH^{initial} = 0.5$. Increasing relative REE fractionation with decreasing pressure is also obvious from distribution coefficients (Fig. 5). From 427 to 362 bar, $K_D^{Lu/La}$ increases about linearly from 1.1 to 2.2 and $K_D^{Gd/La}$ from 1.1 to 1.6. Extrapolation to halite-saturated conditions for the pure NaCl–H_2O system at 250 bar and 52 wt% NaCl in the liquid (Bischoff and Pitzer 1989) would yield an extrapolated $K_D^{Lu/La}$ of about 4 and a $K_D^{Gd/La}$ of about 2.5.

Measured Na and Cl concentrations in quenched vapour shows that HCl is the dominant Cl-bearing vapour species at low pressures, if bulk compositions are very acidic (Fig. 6). At 427 bar, about 0.086 mol Na and 0.097 mol Cl are present, indicating that about 11% of the Cl-bearing species is HCl. As the solvus opens with

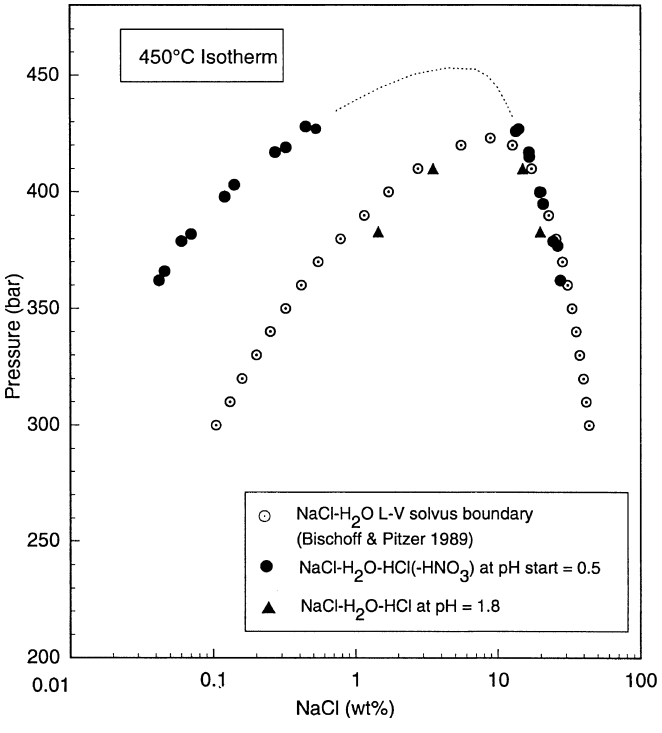

Fig. 1 Pressure–NaCl concentration plot of the NaCl–H_2O and NaCl–H_2O–HCl(–HNO_3) solvi for the 450 °C isotherm at pH 0.5 and 1.8. Values for the NaCl–H_2O system (*open circles*) are from Bischoff and Pitzer (1989); *filled circles* represent our measured NaCl concentrations in brine and vapour of the NaCl–H_2O–HCl system at pH 0.5; *triangles* those at pH 1.8. Values are from Tables 1 and 2

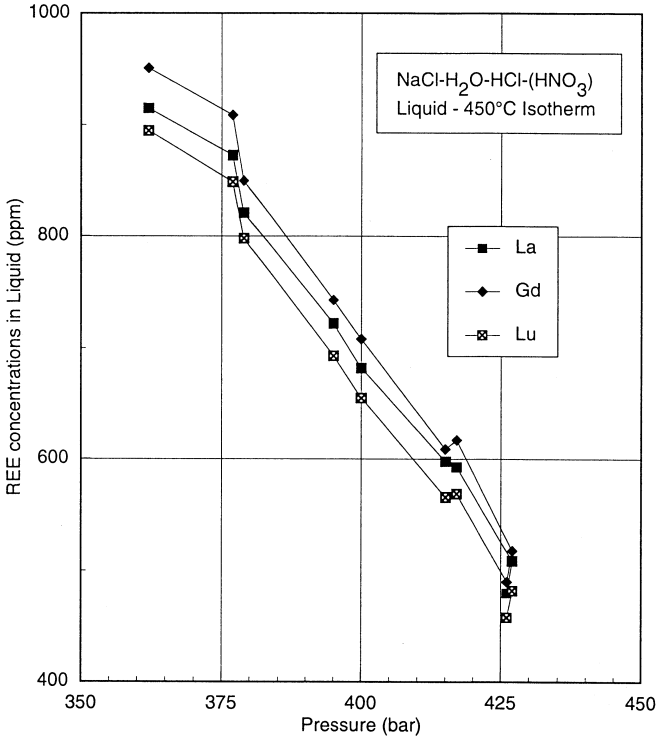

Fig. 2 Concentrations of La, Gd and Lu in the liquid versus pressure for the NaCl–H_2O–HCl(–HNO_3) system at 450 °C and $pH^{initial}$ 0.5. Values are from Table 1

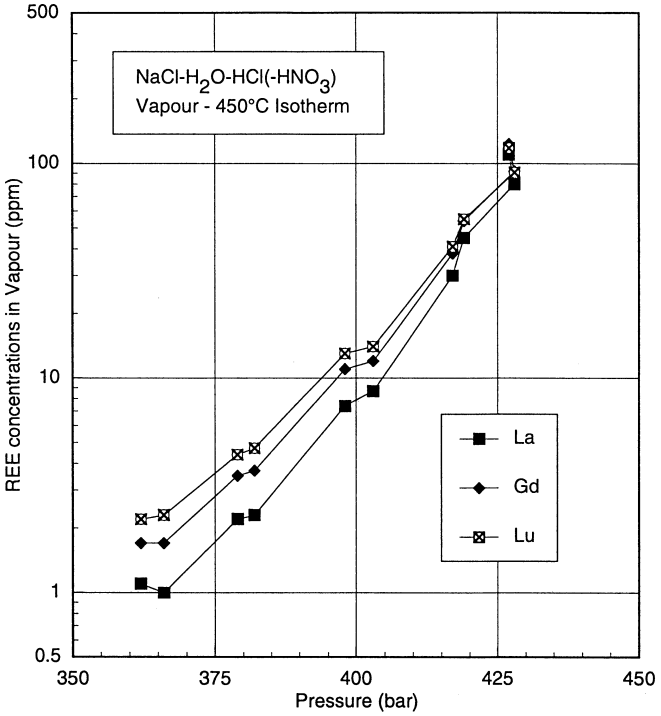

Fig. 3 Concentrations of La, Gd and Lu in the vapour versus pressure for the NaCl–H_2O–HCl(–HNO_3) system at 450 °C and $pH^{initial}$ 0.5. Values are from Table 1

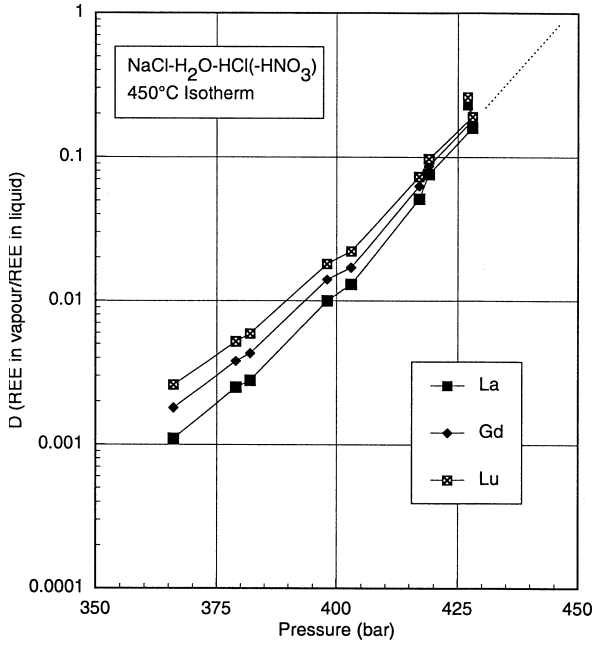

Fig. 4 Partition coefficient $D = C^{vapour}/C^{liquid}$ of La, Gd and Lu versus pressure for the NaCl–H_2O–HCl(–HNO_3) system at 450 °C and $pH^{initial}$ 0.5. Values are from Table 1

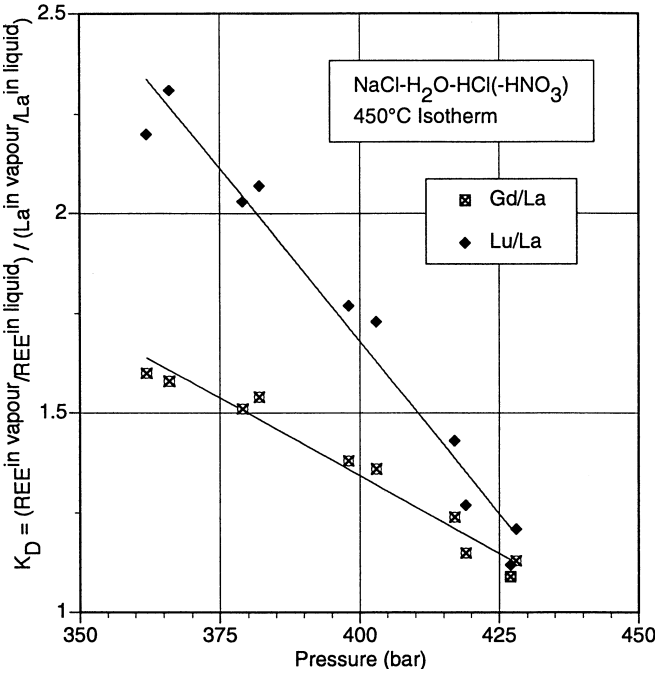

Fig. 5 Distribution coefficient $K_D = (REE^{vapour}/REE^{liquid})/(La^{vapour}/La^{liquid})$ versus pressure of Gd and Lu for the NaCl–H_2O–HCl(–HNO_3) system at 450 °C and $pH^{initial}$ 0.5. Values are from Table 1

decreasing pressure, the Na/Cl ratio changes continuously. At 395 bar, the speciation of Cl is about 50% HCl and 50% NaCl, and at 366 bar to 72% HCl and 28% NaCl (Table 1). The quench-pH of all liquids is less acidic compared with the starting solution and increases from 0.7 to 1.5 as pressure drops and salinity increases. The quench-pH of the vapours is more acidic than the starting solution and ranges between 0.36 and 0.52. This confirms that, to some extent, a hydrolysis reaction of

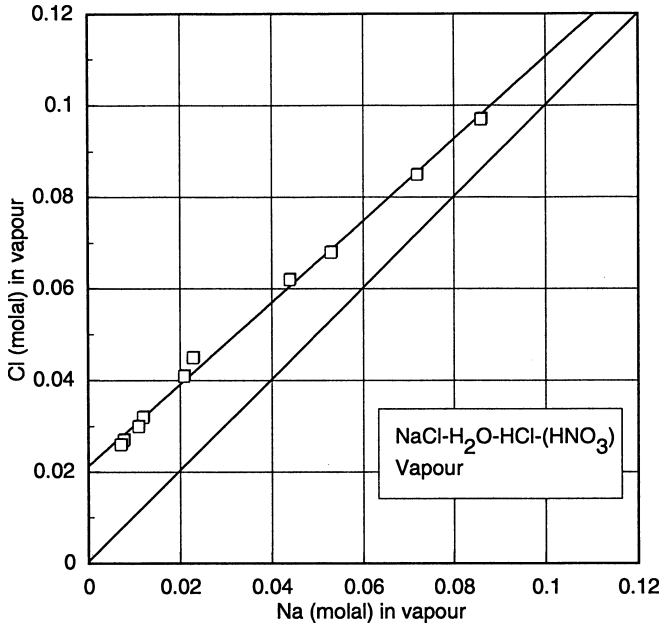

Fig. 6 Na versus Cl concentrations along the vapour limb of the NaCl–H_2O–HCl(–HNO_3) system from 427 to 362 bar at 450 °C and $pH^{initial}$ 0.5. Values are from Table 1

the type NaCl + H_2O = Na(OH) + HCl occurs. The liquid is less acidic because HCl preferentially partitions into the vapour phase. The effect becomes increasingly important with the opening of the solvus towards low pressures. It results from the fact that, due to the very small electrolyte dissociation in the vapour, concentrations of the components NaCl and HCl depend mainly on their own vapour pressures (Shmulovich et al. 1995b; Bischoff et al. 1996).

Fractionations at 350, 400 and 450 °C at pH 1.8

Liquid–vapour fractionation of La, Ce, Eu, Gd, Y, Ho and Lu, along with Na, Cl and quench-pH, has been determined between 141 and 133 bar at 350 °C, between 260 and 242 bar at 400 °C, and for 410 and 383 bar at 450 °C. Results are given in Table 2.

In contrast to the first series of experiments, the starting solution contained very small amounts of REE (~2 ppm). At all conditions, the REE are depleted in the liquid compared with the starting solution. Mass balance estimations have shown that only about 50% of the introduced REE are present for the first liquid + vapour pair, and in the case of Ce, only about 7% (Table 4). Obviously, in this experiment the autoclave wall was incompletely passivated, and about 50% of the initial REE have been lost to the autoclave wall. The effect is very strong for Ce, probably because it is incorporated as CeO_2 into the TiO_2 layer. The decreasing amount of each REE in the liquid with decreasing pressure along the 350 and 400 °C isotherms (Table 2) may result because experiments for a particular isotherm started at high and ended at low pressures. Fluids at low pressure were significantly longer exposed to the autoclave material (see above). REE in the vapour phase are strongly depleted relative to the starting solution, and concentrations decrease drastically towards lower pressure as the solvus opens at a particular isotherm. Quench-pH of liquids except one is between 1.9 and 2.2 and higher than the starting solution and quenched vapours are more acidic with values between 1.2 and 1.6 due to hydrolysis.

Although a large part of the REE in these experiments with low initial REE concentrations has been removed from the liquid–vapour system, it can reasonably be assumed that equilibrium partitioning of the REE between each sampled L–V pair was achieved (see section below). This is shown in Fig. 7a, b for the 450 and 350 °C isotherms, respectively. The corresponding partition coefficients $D = REE^{vapour}/REE^{liquid}$ for La, Gd and Lu show a very similar behaviour as described above, and D-values for Eu, Y and Ho closely follow this trend. Each isotherm is clearly defined by the D-values at particular pressures. D's decrease about one to one and a half orders of magnitude with decreasing

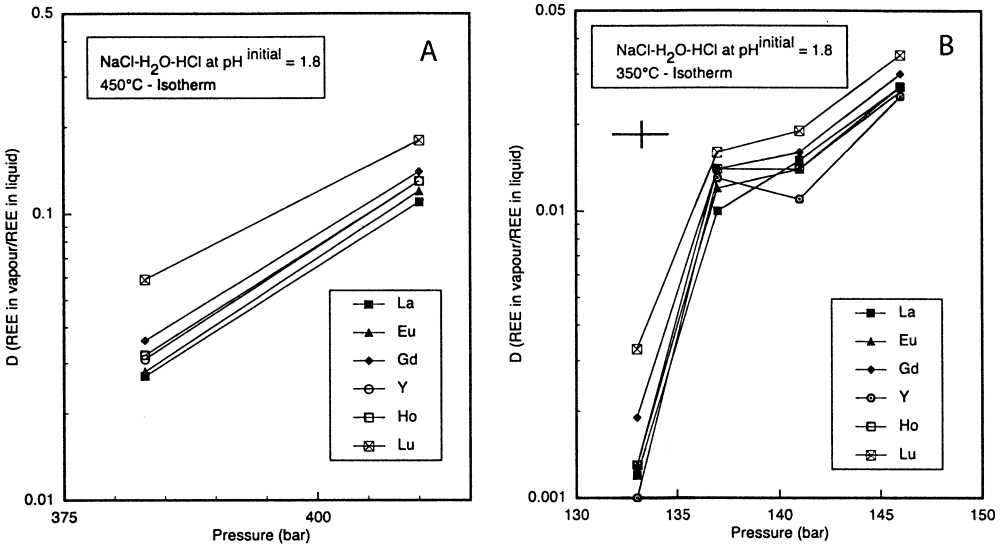

Fig. 7A, B Plots of the partition coefficient $D = C^{vapour}/C^{liquid}$ versus pressure of REE for the NaCl–H_2O–HCl system at $pH^{initial}$ 1.8. **A** 450 °C isotherm, **B** 350 °C isotherm. Values are from Table 2

pressure in the observed pressure ranges (Table 2). Lu always fractionates preferentially into the vapour phase relative to La. The effect is smaller at small total fractionations near the critical points and becomes larger with the opening of the solvus. This is particularly evident for the 350 °C isotherm. At 146 bar, D_{La} is 0.027, $D_{Gd} = 0.030$ and $D_{Lu} = 0.035$. If pressure drops to 133 bar, D_{La} is 0.0012, $D_{Gd} = 0.0019$ and $D_{Lu} = 0.0033$. In this T-region, small pressure changes result in dramatic REE fractionations. At 450 °C and 410 bar, D_{La} is 0.11, $D_{Gd} = 0.14$ and $D_{Lu} = 0.18$; at 450 °C and 383 bar, $D_{La} = 0.027$, $D_{Gd} = 0.036$ and $D_{Lu} = 0.059$ (Fig. 7a). REE partition coefficients are about one order of magnitude higher than those at identical P and T using a starting solution of $pH^{initial}$ 0.5. This effect is discussed below.

The system $CaCl_2$–H_2O–HCl

Liquid–vapour fractionation of the REE and Sr, along with the matrix elements Ca and Cl have been determined for the 400 °C-isotherm at 15 pressures between 298 and 187 bar. Results are presented in Table 3 and Figs. 8, 9, 10, 11, 12 and 13.

Figure 8 shows a pressure versus concentration diagram of the matrix component $CaCl_2$ in coexisting liquid and vapour. $CaCl_2$ concentrations have been calculated from Table 3 assuming that all of the measured Ca in both phases is present as $CaCl_2$. The experimentally determined solvus boundaries for the pure $CaCl_2$–H_2O system (values from Bischoff et al. 1996) are also given. The shapes of the two solvi are slightly different, particularly with respect to the vapour limb. The critical point at 10 wt% $CaCl_2$ for the HCl-bearing system ($pH^{initial}$ 1.8) is at about 300 bar and coincides with that of the pure $CaCl_2$–H_2O system within error limits. In the HCl-bearing system, the solvus is more widely expanded by the vapour limb from 280 bar towards lower pressures. This is an expected behaviour because, at a given salinity of the vapour, the pressure should shift to somewhat higher values because the vapour pressure of HCl is much higher than that of $CaCl_2$. Again, both solvus boundaries are clearly defined by the fractionation of the matrix components $CaCl_2$ and HCl, demonstrating that contamination of the vapour phase by aerosol formation did not occur or was insignificant during sampling.

The concentration of most REE in the liquid increases continuously as pressure drops along the opening solvus from 298 to 253 bar (Table 3). A significant step towards lower concentrations occurs between 253 and 232 bar, accompanied by a strong increase of the pH of the quenched liquid from 7.5 to 10. This is exactly the pressure range where hydrolysis begins to play an important role in the $CaCl_2$–H_2O system for the relevant 400 °C isotherm (Bischoff et al. 1996). The significantly lower REE concentrations below 232 bar and the concomitant increase in the quench-pH are interpreted as a

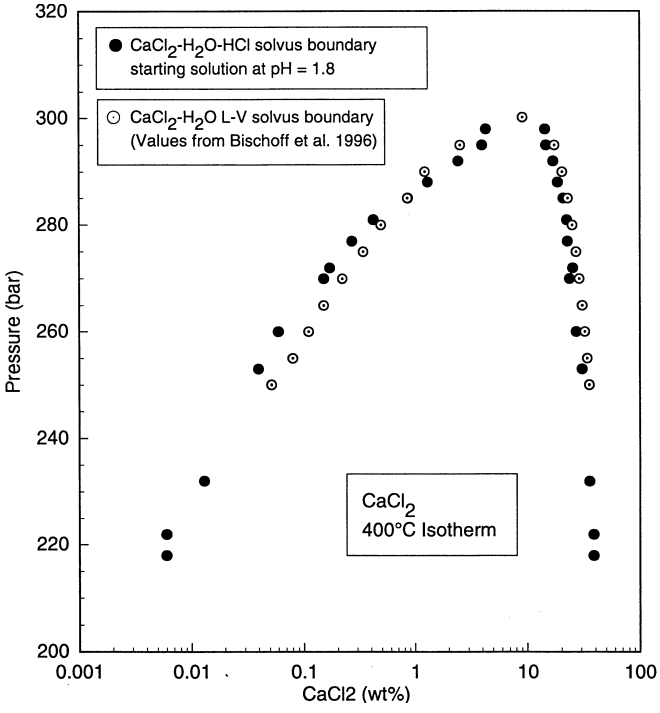

Fig. 8 Pressure–$CaCl_2$ concentration plot of the $CaCl_2$–H_2O and $CaCl_2$–H_2O–HCl ($pH^{initial}$ 1.8) solvi at 400 °C. Values for the $CaCl_2$–H_2O system (*open circles*) are from Bischoff et al. (1996); *filled circles* represent our measured $CaCl_2$ concentrations in brine and vapour of the $CaCl_2$–H_2O–HCl system from Table 3

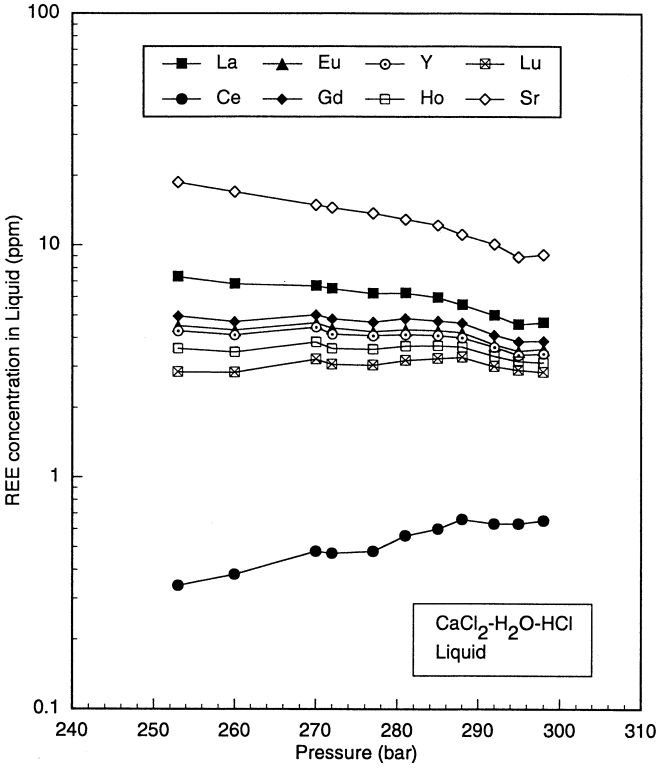

Fig. 9 Plot of REE-concentrations (ppm) in the liquid versus pressure for the $CaCl_2$–H_2O–HCl-system at 400 °C. Values are from Table 3

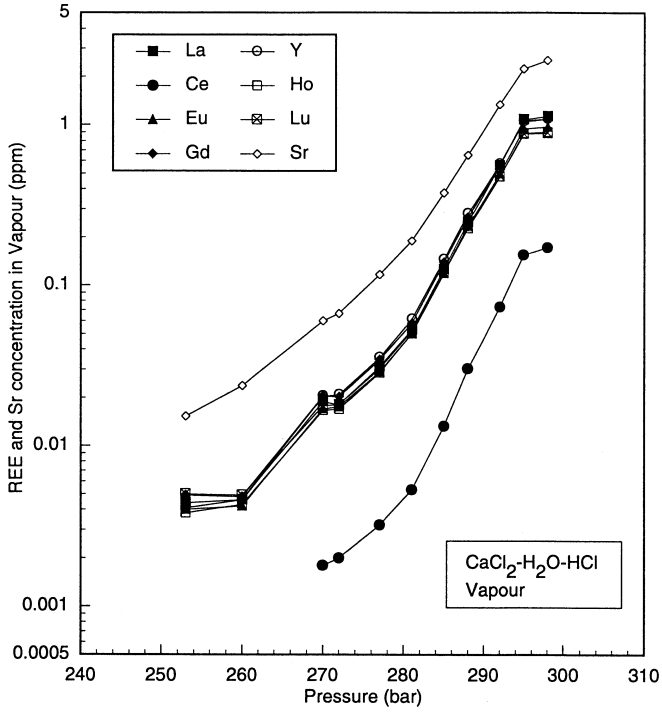

Fig. 10 Plot of REE-concentrations (ppm) in the vapour versus pressure for the $CaCl_2$–H_2O–HCl system at 400 °C. Values are from Table 3. Ce concentrations in the vapour below 270 bar are in the range of the detection limit, therefore, and disregarded

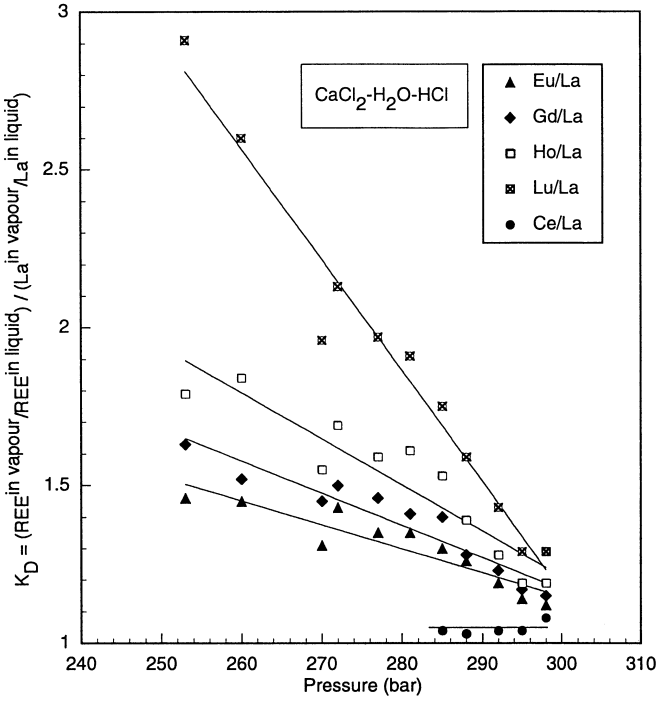

Fig. 12 Plot of the distribution coefficient $K_D = (REE^{vapour}/REE^{liquid})/(La^{vapour}/La^{liquid})$ versus pressure for Ce, Eu, Gd, Ho and Lu for the $CaCl_2$–H_2O–HCl system at 400 °C. Values from Table 3

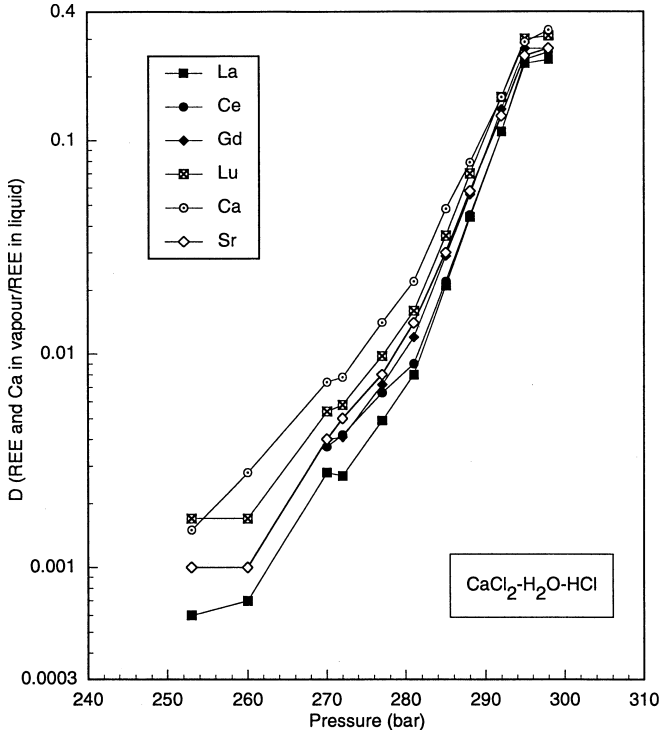

Fig. 11 Plot of the partition coefficient $D = C^{vapour}/C^{liquid}$ for La, Ce, Gd, Lu, Sr and the matrix element Ca versus pressure for the $CaCl_2$–H_2O–HCl system at 400 °C. Values are from Table 3. Ce-concentrations in the vapour below 270 bar are within the analytical detection limits and the respective D-coefficients were disregarded

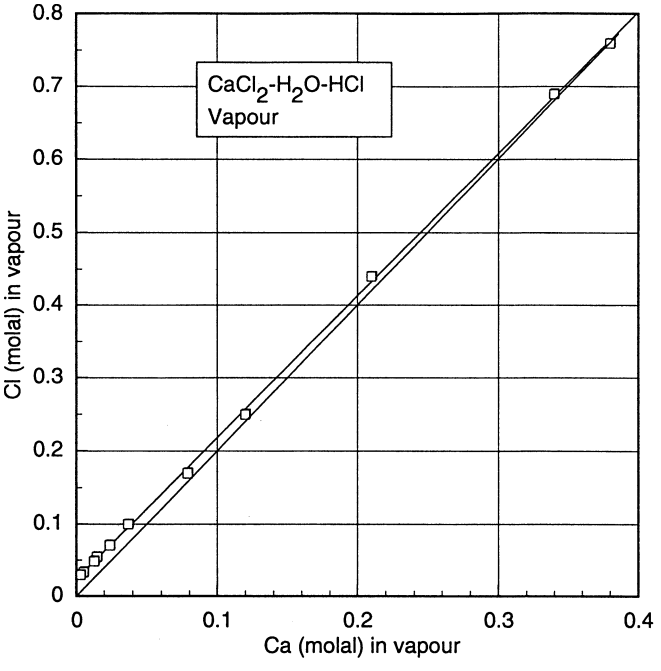

Fig. 13 Plot of Ca versus Cl concentrations along the vapour limb in the $CaCl_2$–H_2O–HCl system from 298 to 253 bar at 400 °C. Values are from Table 3

result of precipitation of $REE(OH)_3$ from the brine. This is in line with arguments of Bischoff et al. (1996) for possible precipitation of $Ca(OH)_2$ from neutral $CaCl_2$–H_2O starting solutions at low pressures. If so,

liquid–vapour partitioning at pressures below 253 bar occurred in presence of solid hydroxides. Equilibrium between vapour, liquid and solids was probably not achieved at these conditions. Therefore, these data are not considered any further in the following.

Figure 9 shows the concentrations of La, Ce, Eu, Gd, Y, Ho, Lu and Sr in the liquid phase with decreasing pressure, equivalent to increasing salinity (Fig. 8). All REE are enriched in the liquid relative to their concentrations in the starting solution, with the exception of Ce. This indicates that, though absolute REE concentrations were again very low, the autoclave surface was far better passivated than in the previous experiments. Concentrations of REE increase continuously as pressure drops along the opening solvus. From 298 to 253 bar, La increases from about 4.7 to 7.3 ppm, Gd from 3.9 to 5.0 ppm, whereas Lu is nearly constant. In the liquid, concentrations of LREE are higher relative to HREE and they increase continuously along the Lu–La suite for each pressure. It is obvious that differences in concentration between LREE and HREE become larger with decreasing pressure. The REE concentration versus pressure curves show a consistent behaviour with the exception of Ce. Ce concentrations in the liquid are between 0.7 and 0.3 ppm, which is far below the starting composition of about 2 ppm. This is again explained by Ce incorporation as CeO_2 component into the protective TiO_2 layer. We cannot exclude that a small part of all other REE might also have been lost into the autoclave material. However, we will show below that this has no significant effect for the REE distributions between liquid and vapour, and that even for Ce, reasonable L–V partition coefficients result. The Sr concentrations in the liquid (Table 3) show a very similar behaviour. Initially present of 4.7 ppm, they increase from about 9.1 to 18.7 ppm as pressure drops from 298 to 253 bar. The pH values of the quenched liquid increase continuously from 2.2 to 5.1 along the same pressure range, equivalent to increasing salinity from 14.4 to 30.7 wt% $CaCl_2$ (see Fig. 8). All quenched liquids are less acidic than the starting solution at pH 1.8 at room temperature.

Figure 10 shows the corresponding REE and Sr concentrations in the vapour phase. All REE are depleted in the vapour relative to their concentrations of about 2 ppm in the starting solution. Near the critical point at 298 bar, concentrations for all REE are about 1 ppm and decrease continuously to about 0.004 ppm at 253 bar by two and a half orders of magnitude with the opening of the solvus. The REE concentration patterns are very similar except for Ce, which shows a parallel pattern at much lower absolute concentrations of 0.17 to 0.0008 ppm. The concentrations of Sr in the vapour show a comparable trend; they decrease from 2.5 to 0.015 ppm as pressure drops from 298 to 253 bar. The pH of all quenched vapours is more acidic than the starting solution. pH values are 1.6 to 1.7: that is constant within error limits.

The corresponding partition coefficients $D = REE^{vapour}/REE^{liquid}$ for selected REE and Sr are presented in Fig. 11 along with D-values of the matrix element Ca. The REE distribution patterns follow broadly that of Ca. D_{Ca} decreases continuously from 0.33 to 1.5×10^{-3}, D_{La} from 0.24 to 0.6×10^{-3}, D_{Gd} from 0.28 to 1×10^{-3} and D_{Lu} from 0.31 to 1.7×10^{-3} as pressure drops from 298 to 253 bar. At each pressure value, the REE are depleted in the vapour phase relative to Ca. The important result is again that the HREE are enriched in the vapour phase relative to the LREE. The effect is small near the critical point ($D_{Lu} = 0.31$, $D_{Gd} = 0.28$; $D_{La} = 0.24$ at 298 bar), but relative fractionation becomes increasingly effective with the opening of the solvus, which is immediately evident from the splitting up of the REE patterns towards lower pressures (Fig. 11). Values of D_{Ce} follow closely that of La and are compatible with the general trend, in spite of the fact that about 80% of the total Ce content in the starting solution was lost to the autoclave wall. Obviously, L–V partitioning of Ce occurred rapidly enough to achieve equilibrium concentrations along the entire pressure range despite of its continuous disappearance from the L–V system during the experiment. Taking the D-pressure curves from 260 to 295 bar for each element (excluding the values at 298 bar) and extrapolating them to a D-value of 1, all curves coincide at 302 ± 2 bar. This defines the critical point of the $CaCl_2$–H_2O–HCl system at 400 °C and $pH^{initial} = 1.8$ and demonstrates internal consistency of the measured P–T–X data. The partitioning behaviour of Sr relative to Ca is also shown in Fig. 11. Sr is depleted in the vapour relative to Ca and its D-value pattern coincides with that of Gd.

The L–V fractionations between selected REE relative to La in terms of distribution coefficients $K_D = (REE^{vapour}/REE^{liquid})/(La^{vapour}/La^{liquid})$ are presented in Fig. 12. K_D's for all REE increase uniformly with increasing atomic number and with decreasing pressure. There is approximately a linear negative correlation of K_D with pressure for each particular REE. Distribution coefficients are close to 1 near the critical point, with $K_D{}^{Lu} = 1.3$ and $K_D{}^{Gd} = 1.2$ at 298 bar. At ~250 bar, Lu is enriched in the vapour relative to La by a factor of about 3, Ho by about 1.8, Gd by 1.6 and Eu by about 1.4. Bearing in mind that in the $CaCl_2$–H_2O system salt saturation is attained at 85 wt% $CaCl_2$ and about 50 bar, the progressive opening of the solvus towards much lower pressures may result in much larger HREE/LREE fractionations between vapour–liquid pairs.

The pH was 1.8 in the homogeneous starting solution of the $CaCl_2$–H_2O–HCl system. Measured pH values of quenched vapours are 1.6 to 1.7 (Table 3). Again, hydrolysis occurred with a reaction of the type $CaCl_2 + H_2O = Ca(OH)_2 + 2HCl$. The liquid is less acidic because HCl preferentially partitions into the vapour phase. The effect becomes increasingly important with the opening of the solvus towards low pressures. Near the critical point, measured Ca and Cl concentrations in the vapour are balanced to form the $CaCl_2$ molecule, whereas at low pressures and lower total concentrations

much more Cl relative to Ca is present (Fig. 13). HCl becomes the major Cl-bearing species in the vapour (see also Bischoff et al. 1996).

Discussion

Fractionation behaviour

The partitioning of REE between liquid and vapour broadly follows the main salt component and described the $D = REE^{vapour}/REE^{liquid}$ values as a function of pressure. Berndt et al. (1996) correlated the liquid–vapour partitioning of D/H isotopes in the NaCl–H_2O system to a ΔP value, which is the difference between the critical and the actual pressure at a given temperature and salinity. Shmulovich et al. (1999) related D/H and $^{18}O/^{16}O$ partitioning in the same system to the salinity of the fluid phase at a given temperature. Both approaches are not appropriate for the systems considered here. The solvus boundary of the vapour depends strongly on bulk pH, whereas that of the liquid does not, and the critical points, therefore, are not very well constrained. In the NaCl-bearing system at 450 °C and $pH^{initial}$ 1.8, the partition coefficients of the REE are about one order of magnitude higher than those determined at identical temperature and pressure at $pH^{initial}$ 0.5 (Tables 1 and 2, Figs. 4 and 7a). This is not surprising because NaCl concentrations in the liquid of the pure NaCl–H_2O and the NaCl–H_2O–HCl at $pH^{initial}$ 1.8 are almost identical at given P and T, whereas the NaCl concentration in the vapour at $pH^{initial}$ 0.5 is about one order of magnitude lower (Fig. 1). The important point is that the relative fractionations in terms of $K_D^{REE/La}$ do not depend on the bulk pH of the system. At 450 °C and the respective pressures, $K_D^{Gd/La}$ and $K_D^{Lu/La}$ coincide in both series of experiments (see Fig. 14 for $K_D^{Lu/La}$). This confirms that pH, total REE concentration in the range of 2 to 310 ppm, and some adsorption of REE at the autoclave material do not change the distribution coefficients significantly.

Figure 14 summarises the L–V fractionation behaviour of REE expressed as $K_D^{Lu/La}$ at 350, 400 and 450 °C for the NaCl–H_2O, and at 400 °C for the $CaCl_2$–H_2O system. At each isotherm, it increases linearly with decreasing pressure: that is with increasing opening of the solvus. At 400 and 450 °C, the intersections of the regression lines with the abscissa at $K_D^{Lu/La} = 1$ define approximately the critical pressures for the respective conditions. This does not hold for the 350 °C isotherm of the NaCl–H_2O system. The reason for this is the behaviour of the vapour limb below the critical point of pure water where at 350 °C NaCl concentrations decrease with increasing pressure between 150 and 165 bar (see Bischoff and Pitzer 1989, their Fig. 7).

Maximum fractionations occur at the maximum opening of the solvus: that is at salt-saturated conditions. In the NaCl-bearing system, salt saturation is attained at 105 bar for 350 °C, at 172 bar for 400 °C and at

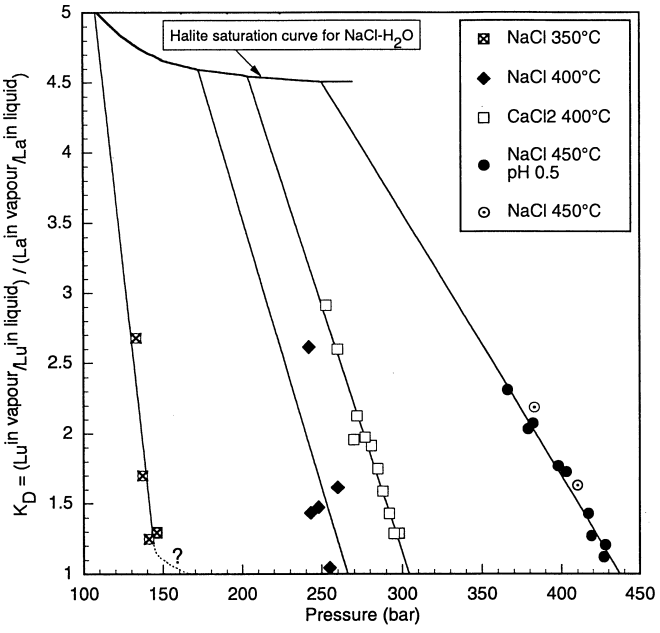

Fig. 14 Distribution coefficient $K_D = (Lu^{vapour}/Lu^{liquid})/(La^{vapour}/La^{liquid})$ versus pressure for the 350, 400 and 450 °C isotherms of the NaCl–H_2O–HCl(–HNO_3) system and for the 400 °C isotherm of the $CaCl_2$–H_2O–HCl system. Values are from Tables 1, 2 and 3. P–T conditions for halite saturation (system NaCl–H_2O) are from Bischoff and Pitzer (1989)

250 bar for the 450 °C isotherm (Bischoff and Pitzer 1989). Extrapolation of the regression lines to pressures of salt saturation shows that $K_D^{Lu/La}$ is 5.1 at 350 °C, 4.6 at 400 °C and 4.5 at 450 °C (Fig. 14). An almost identical $K_D^{Lu/La}$ value of 5 ± 0.5 results at salt saturation, irrespective of temperature. It can reasonably be assumed that this holds also for isotherms at higher temperatures because these also end somewhere on the extension of the halite saturation curve towards higher pressure. This is supported by the analogous fractionation behaviour of D/H and $^{18}O/^{16}O$ isotopes between liquid and vapour in the H_2O–NaCl system (Shmulovich et al. 1999). Maximum fractionations of 28‰ in $D/H_{(V-L)}$ and about 2‰ in $^{18}O/^{16}O_{(L-V)}$ result along the liquid + vapour + halite curve and are about constant over the temperature range from 350 to 600 °C. The effect is produced by two factors that move in opposite directions. In principle, higher temperature favours less fractionation, but also implies, at salt-saturation, higher salinities in the liquid and lower ones in the vapour, which opens the solvus more widely (Sourirajan and Kennedy 1962; Bischoff and Pitzer 1989). The result is an increasing difference in density between both phases, which enhances fractionation. Obviously, both factors counterbalance over a large temperature range. If one follows this speculation, it would mean that a $K_D^{Lu/La}$ value of about 5 is also valid for the 500 °C and possibly also for the 600 °C isotherm of the H_2O–NaCl system. It is clear that these extrapolations must be considered with caution. It is possible that, at low pressure and high salinity of the liquid, hydrolysis induced a high pH in the liquid. As

a consequence, precipitation of $REE(OH)_3$ would occur, thus removing the REEs from the liquid–vapour system even at low total concentrations.

At 400 °C, salt saturation in the $CaCl_2$–H_2O system would be attained at about 50 bar and 85 wt% $CaCl_2$ (Shmulovich et al. 1995a). A tentative extrapolation results in $K_D^{Lu/La}$ of about 10 at these conditions. Our results suggest, however, that hydrolysis of $CaCl_2$ and precipitation of $Ca(OH)_2$ and co-precipitation of $REE(OH)_3$ become indeed effective in this system at about 250 bar and below (see also Bischoff et al. 1996). This is strongly supported by decreasing REE concentrations in the liquid below 253 bar. As a result, calculated $K_D^{REE/La}$ values also decrease. This is not an artefact of the extremely low REE concentrations in the vapour at low pressure because the lowest measured concentrations were still 10 to 50 times higher than the experimental blank. Precipitation is the result of a complex process involving hydrolysis due to

$$MeCl_x + xH_2O = Me(OH)_x + xHCl \quad (2)$$

fractionation of hydrolysis products between liquid and vapour, precipitation of $Ca(OH)_2$ and co-precipitation of $REE(OH)_3$. The products of the hydrolysis reaction are distributed between liquid and vapour very differently, in such a way that HCl is partitioned mainly into the vapour and $Me(OH)_x$ preferentially into the brine. The effect increases towards lower pressures (Figs. 6 and 13) and is additionally enhanced by our sampling method, which produced more vapour relative to liquid at each sequential sampling step along a particular isotherm. This may have resulted in saturation of hydroxides if they have a small solubility. This is not possible for NaOH, but was obviously realised for $Ca(OH)_2$ and $REE(OH)_3$ in the Ca-bearing system.

That HREE in water–salt systems are preferentially fractionated into the vapour has some similarities to other systems. Experimental work above 1,000 K (Poliachonok 1972) has shown that the vapour pressures of $REECl_3$ systematically increase from $LaCl_3$ to $LuCl_3$, and YCl_3 also fits into this pattern. Also, a similar dependence on fugacity along the lanthanoid sequence is given by the boiling points of the $REECl_3$. Boiling temperatures at 1 bar systematically decrease from $LaCl_3$ (1,750 °C) to $LuCl_3$ (1,450 °C), indicating that in any mixture at constant temperature the compound with the lower boiling temperature will have the higher vapour pressure. Hence, preferential partitioning of HREE over LREE into the vapour also exists in this system. If this behaviour is transferred to our water–salt system one might argue that also in our case REE fractionation would depend on fugacity of the species, and evaporation of REE would be proportional to their vapour pressure. The argument holds only if similar speciations of REE in both phases exist, which is questionable, even if one considers that the density of the vapour phase in our experiments is still relatively high, and if the interaction for the REE species with the matrix would be the same. It is rather suggested that the fractionation would probably depend mainly on the REE species in the vapour. However, any properties in the vapour are non-linear functions of P, T and composition and, to our knowledge, there are no equations of state and thermodynamic databases currently available that would predict this fractionation behaviour at liquid–vapour conditions.

Speciation of REE in the vapour phase

Very little is known about the speciation of REEs in high salinity brines. Polynuclear species probably prevail. In the vapour, neutral species dominate. We have shown for the H_2O–NaCl–HCl system that at 450 °C and $pH^{initial}$ 1.8 the partition coefficients of the REE are about one order of magnitude higher than those determined at identical temperature and pressure at $pH^{initial}$ 0.5. The REEs are increasingly rejected from vapourisation with increasing acidity of the vapour. Obviously, a hydrolysis process is operating that allows some speculation on the dominant REE species in the vapour phase. We demonstrate this by comparing the measured REE concentrations and quench-pHs of experiments 6 (at 450 °C, 383 bar, $pH^{initial} = 1.8$, $REE^{initial} = 2$ ppm) with that of experiment R7 (at 450 °C, 382 bar, $pH^{initial} = 0.5$, $REE^{initial} = 312$ ppm). P–T conditions are identical within error limits, and pH and total concentrations are distinctly different. Several chemical equilibria between REE species in both liquid and vapour phases were considered out of which the most favourable is discussed.

It can reasonably be assumed that the predominant cation species in the vapour phase are neutral complexes due to the low dielectric constant of water at low densities. A possible hydrolysis reaction between liquid and vapour is then given by

$$REE(OH)_m Cl_n^{liquid} + H_2O^{liquid} \Leftrightarrow REE(OH)_{m+1} Cl_{n-1}^{vapour} + HCl^{vapour} \quad (3)$$

Equilibrium for (1) at constant P and T is expressed as

$$Q = \frac{\left[REE(OH)_{m+1}Cl_{n-1}\right]^{vapour} p_{HCl}}{\left[REE(OH)_m Cl_n\right]^{liquid}} \quad (4)$$

where $REE(OH)_{m+1}Cl_{n-1}^{vapour}$/ $REE(OH)_m Cl_n^{liquid}$ is assumed to be the measured partition coefficient and

$$p_{HCl} = \frac{10^{-pH}}{55.5} \bullet \frac{1}{\rho} \quad (5)$$

pH is the measured quench-pH in the vapour, ρ the density of the quenched vapour and the value of 55.5 are mol of H_2O per kg quenched fluid. If reaction (3) describes hydrolysis correctly, similar Q-values for the two experiments must result. Table 5 shows that Q-values of La, Gd and Lu are in fact similar for runs 6 and R7 whereas for runs R6 (398 bar) and R8 (366 bar) they are not. At identical conditions, corresponding values are obtained for experiments that differ in total REE

Table 5 Q-values of La, Gd and Lu for different pressures and different pH at the 450 °C isotherm of the NaCl–H_2O–HCl system, calculated with Eqs. (4) and (6). For a further explanation, see the text

Run no.	6	R7	R6	R9
Pressure (bar)	383	382	398	366
Quench-pH^{vapour}	1.6	0.5	0.5	0.5
Density (g/ml)	1.15	1.014	1.02	1.008
p^{HCl}	3.94×10^{-4}	5.62×10^{-3}	5.58×10^{-3}	5.65×10^{-3}
D_{La}	0.027	0.0028	0.010	0.0011
D_{Gd}	0.036	0.0048	0.014	0.0018
D_{Lu}	0.059	0.0059	0.018	0.0026
Q_{La} [Eq. (4)]	$\mathbf{1.06\times10^{-5}}$	$\mathbf{1.57\times10^{-5}}$	5.58×10^{-5}	6.21×10^{-6}
Q_{Gd} [Eq. (4)]	$\mathbf{1.42\times10^{-5}}$	$\mathbf{2.70\times10^{-5}}$	7.82×10^{-5}	1.02×10^{-5}
Q_{Lu} [Eq. (4)]	$\mathbf{2.33\times10^{-5}}$	$\mathbf{3.32\times10^{-5}}$	1.00×10^{-4}	1.45×10^{-5}
Q_{La} [Eq. (6)]	4.2×10^{-9}	8.8×10^{-8}	3.1×10^{-7}	3.5×10^{-8}
Q_{Gd} [Eq. (6)]	5.6×10^{-9}	1.5×10^{-7}	4.4×10^{-7}	5.7×10^{-8}
Q_{Lu} [Eq. (6)]	9.2×10^{-9}	1.9×10^{-7}	5.6×10^{-7}	8.3×10^{-8}

abundances. It is ascertained that the predominant REE-bearing species in the vapour are of the type $REECl_{3-n}(OH)_n$ with $n \approx 1$. Ionisation of the dissolved species in the liquid does not invalidate the results.

If it is alternatively assumed that the dominant species in vapour were of the type REEOCl it would follow that the liquid is dominated by species of the type RE-$E(OH)Cl_2$ or their dissociation products, i.e. RE-$E(OH)_2^+$, $REE(OH)Cl^+$ and $REECl_2^+$. The mixed complexes have not been considered in the database of Haas et al. (1995). However, complexes of the type $REECl_2^+$, $REECl^{2+}$ and $REE(OH)^{2+}$ do exist. The stability constants of the chloro-complexes are almost the same for all REE whereas that of the hydroxy-complexes increase from La to Lu. This might be taken as a hint that the assumed species do occur under our experimental conditions.

We also tested the reaction

$$REECl_3^{liquid} + 1H_2O^{liquid} \Leftrightarrow REEOCl^{vapour} + 2HCl^{vapour} \quad (6)$$

Calculated Q-values for Eq. (6) give far less consistent results (Table 5). However, the experiment with $pH^{initial}$ 0.5 shows Q-values for Eq. (3) that are 20–30% higher than those at $pH^{initial}$ 1.8. This might indicate enhanced hydrolysation with some contribution of REEOCl in the vapour. That HREE are preferentially fractionated over LREE into the vapour phase at all conditions is possibly the result of their different hydrolysis behaviour. Increasing Q-values from La to Lu could indicate either increasing contribution of the REEOCl complex as the ionic radius of the REE decreases, or increasing stability constants of the $REECl_2(OH)$ complex in the vapour phase.

Geological implications

Two immiscible fluids, brine and vapour, are often present in the early stages of an evolving hydrothermal system. Fluid inclusion studies have shown that brine inclusions, which were salt-saturated during their formation, are widespread and that the dominant salt species is commonly NaCl (e.g. Roedder 1979, 1984; Reynolds and Beane 1985; Hedenquist et al. 1998). This has been demonstrated for many rocks around shallow intrusions and particularly for porphyry copper deposits (e.g. Bodnar 1995). A fluid-saturated magma may simultaneously exsolve high-salinity brine and vapour, if pressure is low enough (Shinohara et al. 1989; Candela 1991; Shinohara 1994; Williams et al. 1995). Even if early fluids are single phase, successive crystallisation produces a higher salinity fluid, which may intersect the two-fluid solvus easily. If this is accompanied by a concomitant pressure drop, the solvus is struck even more rapidly (Cline and Bodnar 1991, 1994).

Liquid–vapour separation within a hydrothermal system is not restricted to magmatic fluids. Salt-bearing fluids of meteoric or seawater origin may undergo the same boiling process. If cold fluid moves towards an intrusion at depths, it is heated and ascends towards the surface (Cathles 1977). Isobaric heating and subsequent decompression leads into the liquid–vapour immiscibility field. It is clear that any mixture of magmatic and meteoric fluid may experience the same boiling during ascent, heating and depressurisation.

The effect of changing conditions in a NaCl-dominated shallow hydrothermal system on the position of the two fluid solvus and the concomitant REE fractionations is shown in Fig. 15. The illustration is somewhat

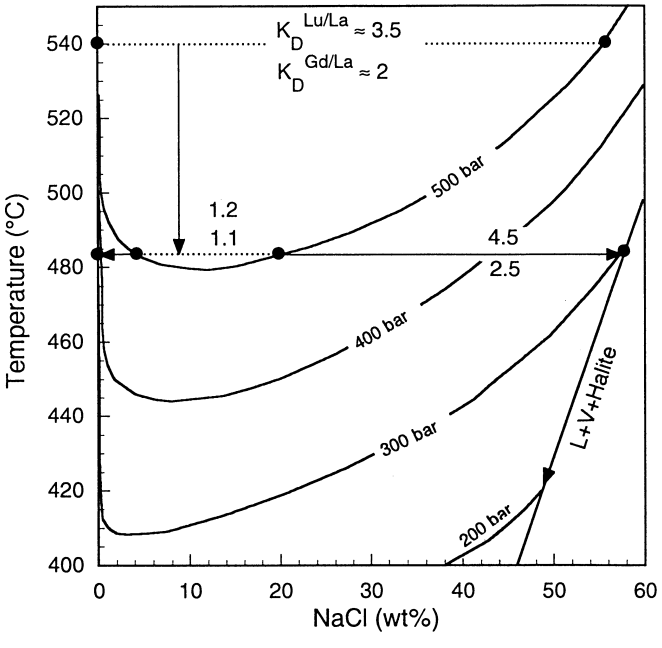

Fig. 15 Solvus boundaries of the system NaCl–H_2O with isobars from 200 to 500 bar illustrating isobaric cooling and isothermal heating for L–V fractionation of REE. $K_D^{Lu/La}$ and $K_D^{Gd/La}$ values were tentatively extrapolated to higher temperatures. Isobaric cooling generates decreasing, isothermal heating increasing fractionations. The concomitant temperature and pressure drop along the halite saturation curve keeps fractionation almost constant at maximum values

simplistic because the solvus boundaries are given for the pure NaCl–H_2O system and the experimentally determined values for $K_D^{Lu/La}$ and $K_D^{Gd/La}$ are in part extrapolated to higher temperatures. The main features remain, however, unchanged. Isobaric cooling of any liquid–vapour system results in strongly reduced fractionation (see also Shmulovich et al. 1999). This is simply because the solvus closes drastically. For example, at 500 bar and 540 °C, $K_D^{Lu/La}$ is about 3,5 and $K_D^{Gd/La}$ about 2. Isobaric cooling to 485 °C results in very small fractionations of $K_D^{Lu/La} \approx 1.2$ and $K_D^{Gd/La} \approx 1.1$. Upon further cooling, the system is driven into the one phase-field. By contrast, isobaric heating of only a few tens of degrees may open the solvus widely, thus forcing fractionations to a maximum. Enhanced opening of the solvus is also produced by isothermal or adiabatic decompression. If the system at 485 °C is isothermically decompressed from 500 to 300 bar, salt is precipitated and fractionation values are shifted from very small to maximum values of about 4.5 for $K_D^{Lu/La}$ and 2.5 for $K_D^{Gd/La}$ (Fig. 15). Any fluid system that evolves along the halite saturation curve is subject to maximum fractionations, irrespective of temperature. At the roof of a shallow intrusion, a complex interplay between open and closed system behaviour develops (e.g. Fournier 1987). Vapour may separate and escape through cavities. Fractionation is then controlled most likely by a Rayleigh fractionation process, which results in even larger overall fractionation effects.

Brines with $CaCl_2$ as predominant salt species are common in sedimentary basins. They have also been found in deep drill holes such as the KTB well (Möller et al. 1997) and seafloor hydrothermal systems (Vanko et al. 1992), and are interpreted to have formed by Ca–Na exchange between brine, plagioclase and mafic minerals at moderate and low temperature. Bischoff et al. (1996) have shown that hydrolysis of $CaCl_2$ due to the reaction

$$CaCl_2 + 2H_2O = Ca(OH)_2 + 2HCl \quad (7)$$

is a geologically important process, where $Ca(OH)_2$ is enriched in the brine and HCl in the conjugate vapour. In a boiling $CaCl_2$–H_2O system in the relevant P–T range where a Rayleigh distillation process is operating, precipitation of $Ca(OH)_2$ probably occurs before salt saturation in the liquid is attained and simultaneous precipitation of $REE(OH)_3$ is most likely. Our data have shown that, at 400 °C, the latter occurred at a pressure somewhere between 253 and 232 bar, equivalent to a salinity of the brine of >35 wt% $CaCl_2$. Therefore, extrapolation of K_D^{REE}'s to salt saturation in this system is unreasonable.

The evolution of REE concentrations in brine and vapour for a boiling $CaCl_2$-bearing system at 400 °C during depressurisation along our experimental pressure range is shown in Fig. 16. REE concentrations are normalised to the matrix element Ca. REE/Ca patterns are calculated assuming that Rayleigh distillation starts at 295 bar (fraction of residual liquid F is 1) and ends at

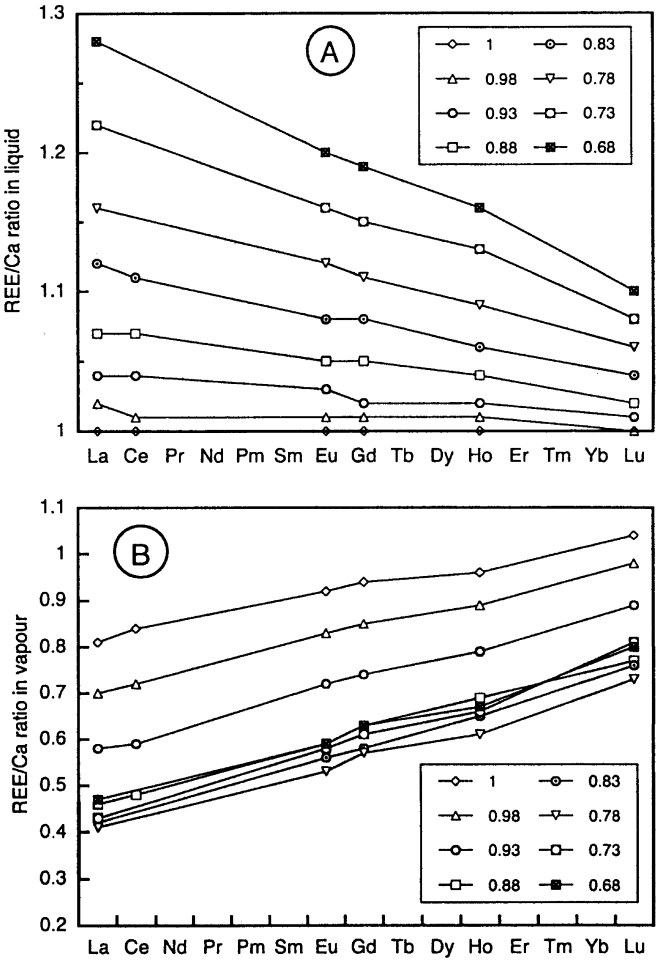

Fig. 16A, B Evolution of REE concentrations in brine and vapour relative to the matrix component, Ca, at 400 °C and decreasing pressure. Patterns are calculated using values from Table 3 by applying Rayleigh distillation that operates from starting conditions at 298 bar where fraction of residual liquid (F) is 1 to 263 bar (F is 0.68). Calculation includes varying K_D's within this range. **A** REE/Ca-ratio in liquid and **B** in vapour versus REE at different fractions of residual liquid

270 bar (fraction of residual liquid F is 0.68), and by using pressure-dependent distribution coefficients $K_D = (REE^{vapour}/REE^{liquid})/(Ca^{vapour}/Ca^{liquid})$ from values in Table 3. It is assumed that 5% of the initial liquid evaporates in each pressure increment. Figure 16A, B illustrates the changes in REE distribution patterns in the liquid and vapour phase, respectively. For F = 1, i.e. just at the beginning of distillation, the differential fractionation corresponds with the K_D values derived from Table 1 at 295 bar. The decrease of REE in the vapour and increase in the brine relative to Ca is obvious, but the increase of the fractionation effect with increasing distillation is small. At F = 1, Lu/Ca and La/Ca ratios in the vapour are 1.04 and 0.81, and at F = 0.68, they are 0.75 and 0.45, respectively. It is clear that large relative fractionations are only expected at

more enhanced distillation, i.e. near salt-saturated conditions.

A hydrothermal Ca-bearing mineral crystallising from a boiling $CaCl_2$-dominated brine should, in principle, display REE patterns as shown in Fig. 16A, provided that no additional REE fractionation between solid and brine occurred. Patterns with decreasing concentrations from La to Lu are well known for hydrothermal fluorite or calcite (i.e. Möller 1983). These trends are, however, commonly much more pronounced with values of relative LREE-HREE fractionations in the range of one order of magnitude. Any possible boiling effect on REE fractionation is masked by much larger fractionations between brine and solids of the coexisting mineral assemblage. Similar arguments hold for mineral precipitation from the vapour phase. Therefore, it might be difficult to prove whether or not gaseous transport of REE played a specific role in the formation of hydrothermal minerals or ore deposits, except in cases where the major part of the liquid is volatilised. The effect may be recognised in hydrothermal systems that drove to salt-saturated conditions, particularly in Na-dominated systems where precipitation of NaOH does not occur and that of $REE(OH)_3$ is unlikely.

Acknowledgements The help of R. Schulz during setting up the Ti-autoclave at GFZ Potsdam is greatly appreciated. Thanks go also to B. Richtert for pH determinations and Cl titration. Drs. D. Vanko and A. Liebscher critically read an earlier version of the manuscript, which is gratefully acknowledged.

References

Berndt ME, Seyfried WE (1997) Calibration of Br/Cl fractionation during subcritical phase separation of seawater: possible halite at 9 to 10°N East Pacific Rise. Geochim Cosmochim Acta 61:2849–2854

Berndt ME, Seal RR, Shank WC, Seyfried WE (1996) Hydrogen isotope systematics of phase separation in submarine hydrothermal systems: experimental calibration and theoretical models. Geochim Cosmochim Acta 60:1595–1604

Bischoff JL, Pitzer KS (1989) Liquid–vapor relations for the system NaCl–H_2O: summary of the P–T–*x* surface from 300° to 500 °C. Am J Sci 289:217–248

Bischoff JL, Rosenbauer RJ, Fournier RO (1996) The generation of HCl in the system $CaCl_2$–H_2O: vapour–liquid relations from 380–500 °C. Geochim Cosmochim Acta 60:7–16

Blundy JD, Wood BJ (1994) Prediction of crystal-melt partition coefficients from elastic moduli. Nature 372:452–454

Bodnar RJ (1995) Fluid inclusion evidence for a magmatic source for metals in porphyry copper deposits. In: Thompson JFH (ed) Magmas, fluids and ore deposits. Mineral Assoc Can Short Course 23:139–152

Candela PA (1991) Physics of aqueous phase evolution in plutonic environments. Am Mineral 76:1081–1091

Cathles LM (1977) An analysis of the cooling of intrusives by ground-water convection which includes boiling. Econ Geol 72:804–826

Cline JS, Bodnar RJ (1991) Can economic porphyry copper mineralization be generated by a typical calc-alkaline melt? J Geophys Res 96(B5):8113–8126

Cline JS, Bodnar RJ (1994) Direct evolution of a brine from a crystallizing silicic melt at the Questa, New Mexico, molybdenum deposit. Econ Geol 89:1780–1802

Driesner T (1997a) Aspects of stable isotope fractionation in hydrothermal solutions. PhD Thesis, ETH Zürich, no 11839, Zürich

Driesner T (1997b) The effect of pressure on deuterium–hydrogen fractionation in high-temperature water. Science 277:791–794

Fournier RO (1987) Conceptual models of brine evolution in magmatic–hydrothermal systems. In: Decker RW, Wright TL, Stauffer PH (eds) Volcanism in Hawaii. US Geol Survey Prof Pap 1350:1487–1506

Haas JR, Shock EL, Sassani DC (1995) Rare earth elements in hydrothermal systems: estimates of standard partial molal thermodynamic properties of aqueous complexes of the rare earth elements at high pressures and temperatures. Geochim Cosmochim Acta 59:4329–4350

Hedenquist JW, Arribas A, Reynolds TJ (1998) Evolution of an intrusion-centered hydrothermal system, far southeast-Lepanto porphyry and epithermal Cu–Au deposits, Philippines. Econ Geol 93:373–404

Heinrich CA, Günther D, Prince C, Schäfer B, Stalder R (1999) Excimer laser-ablation ICP-MS Microanalysis: studies of element-distribution among fluids, minerals and melts in natural and experimental systems [Abstr]. EOS Trans Am Geophys Union 80(17):361

Horita J, Cole DR, Wesolowski DJ (1995) The activity–composition relationship of oxygen and hydrogen isotopes in aqueous salt solutions: III Vapor–liquid water equilibration of NaCl solutions to 350 °C. Geochim Cosmochim Acta 59:1139–1151

Möller P (1983) Lanthanoids as a geochemical probe and problems in lanthanoid geochemistry: distribution and behaviour of lanthanoids in non-magmatic phases. In: Sinha (ed) Systematics and the properties of the lanthanides. Reidel, Amsterdam, pp 561–616

Möller P, Weise SM, Althaus E, Bach W, Behr HJ, Borchardt R, Bräuer K, Drescher J, Erzinger J, Faber E, Hansen BT, Horn EE, Huenges E, Kämpf H, Kessels W, Kirsten T, Landwehr D, Lodemann M, Machon L, Pekdeger A, Pielow HU, Reuthel C, Simon K, Walther J, Weinlich FH, Zimmer M (1997) Paleofluids and recent fluids in the upper continental crust: results from the German Continental Deep Drilling Program (KTB). J Geophys Res 102(B8):18233–18254

Poliachonok OG (1972) The problems of energetic and stability of vapourized halogenides. PhD Thesis, Faculty of Inorganic Chemistry, University of Leningrad

Reynolds TJ, Beane RE (1985) Evolution of hydrothermal fluid characteristics at the Santa Rita, New Mexico, porphyry copper deposit. Econ Geol 80:1228–1347

Roedder E (1979) Fluid inclusions as samples of ore fluids. In: Barnes HL (ed) Geochemistry of hydrothermal ore deposits, 2nd edn. Wiley, New York, pp 684–737

Roedder E (1984) Fluid inclusions. Mineral Soc Am, Rev Mineral, vol 16

Shinohara H (1994) Exsolution of immiscible vapor and liquid phases from a crystallizing silicate melt: Implications for chlorine and metal transport. Geochim Cosmochim Acta 58:5215–5221

Shinohara H, Iiyama JT, Matsuo S (1989) Partition of chlorine compounds between silicate melts and hydrothermal solutions: I. Partition of NaCl–KCl. Geochim Cosmochim Acta 53:2617–2630

Shmulovich KI, Tkachenko SI, Plyasunova NV (1995a) Phase equilibria in fluid systems at high pressures and temperatures. In: Shmulovich KI, Yardley BWD, Gonchar GG (eds) Fluids in the crust. Chapman and Hall, London, pp 193–214

Shmulovich KI, Sorokin VI, Zaraisky GP (1995b) Hydrothermal experimental techniques used at the Institute of Experimental Mineralogy, Russian Academy of Sciences. In: Shmulovich KI, Yardley BWD, Gonchar GG (eds) Fluids in the crust. Chapman and Hall, London, pp 43–56

Shmulovich KI, Landwehr D, Simon K, Heinrich W (1999) Stable isotope fractionation between liquid and vapour in water–salt systems. Chem Geol 157:343–354

Sourirajan S, Kennedy GC (1962) The system H_2O–NaCl at elevated temperatures and pressures. Am J Sci 260:115–141

Spivack AJ, Berndt ME, Seyfried Jr WE (1990) Boron isotope fractionation during supercritical phase separation. Geochim Cosmochim Acta 54:2337–2339

Vakulenko AG, AlekhinYu V, Razina MV (1989) Solubility and thermodynamic properties of alkali chlorides in steam. Proceedings of the II International Symposium on Properties of Water and Steam. Prague, pp 395–401

Vanko D, Griffith JD, Erickson CL (1992) Calcium-rich brines and other hydrothermal fluids in fluid inclusions from plutonic rocks, Oceanographer transform, Mid-Atlantic Ridge. Geochim Cosmochim Acta 56:35–47

Williams TJ, Candela PA, Piccoli PM (1995) The partitioning of copper between silicate melts and two-phase aqueous fluids: an experimental investigation at 1 kbar, 800 °C and 0.5 kbar, 850 °C. Contrib Mineral Petrol 121:388–399